Downloaded from jnm.snmjournals.org by on October 29, 2018. For personal use only.
Journal of Nuclear Medicine, published on September 20, 2018 as doi:10.2967/jnumed.118.212720

Synthesis and preclinical characterization of the PSMA-targeted hybrid tracer PSMA-I&F for nuclear and fluorescence imaging of prostate cancer

Margret Schottelius*[1], Alexander Wurzer[1], Katharina Wissmiller[1], Roswitha Beck[1], Maximilian Koch[2], Dimitrios Gkorpas[2], Johannes Notni[1], Tessa Buckle[3], Matthias N. van Oosterom[3], Katja Steiger[4], Vasilis Ntziachristos[2], Markus Schwaiger[5], Fijs W.B. van Leeuwen[3], Hans-Jürgen Wester[1]

[1] Chair for Pharmaceutical Radiochemistry, Technische Universität München, Walther-Meissner-Strasse 3, 85748 Garching, Germany

[2] Chair for Biological Imaging (CBI), Technische Universität München, Trogerstr. 9, 81675 Munich, and Institute for Biological and Medical Imaging (IBMI), Helmholtz Centre Munich, Ingolstaedter Landstraße 1, 85764 Oberschleißheim, Germany

[3] Interventional Molecular Imaging Laboratory, Department of Radiology, Leiden University Medical Center, Albinusdreef 2, 2333 ZA Leiden, The Netherlands

[4] Institute for Pathology, Klinikum rechts der Isar, Technische Universität München, Ismaningerstr. 22, 81675 Munich, Germany

[5] Department of Nuclear Medicine, Klinikum rechts der Isar, Technische Universität München, Ismaningerstr. 22, 81675 Munich, Germany

* to whom correspondence should be addressed

Prof. Dr. Margret Schottelius
Chair for Pharmaceutical Radiochemistry
Technische Universität München
Walther-Meissner-Strasse 3
85748 Garching, Germany
m.schottelius@tum.de
Phone 0049 89 289 12258
Fax 0049 89 289 12204

Running title: Optical/nuclear imaging using PSMA-I&F
Word count (w/o abstract)**:** 5878

Immediate Open Access: Creative Commons Attribution 4.0 International License (CC BY) allows users to share and adapt with attribution, excluding materials credited to previous publications.
License: https://creativecommons.org/licenses/by/4.0/.
Details: http://jnm.snmjournals.org/site/misc/permission.xhtml.

Downloaded from jnm.snmjournals.org by on October 29, 2018. For personal use only.

ABSTRACT

The PSMA-targeted radiotracers ^{68}Ga/^{177}Lu-PSMA-I&T and ^{99m}Tc-PSMA-I&S are currently successfully employed for clinical PET imaging, radionuclide therapy and radioguided surgery of metastatic prostate cancer. To additionally exploit the high sensitivity and spatial resolution of fluorescence imaging for improved surgical guidance, a first PSMA-I&T-based hybrid tracer, PSMA-I&F (DOTAGA-k(Sulfo-Cy5)-y-nal-k-Sub-KuE), has been developed and evaluated.

The in vitro PSMA-targeting efficiency of PSMA-I&F, the reference PSMA-I&T and their corresponding ^{nat}Ga-/^{68}Ga- and ^{nat}Lu/^{177}Lu-counterparts was determined in LNCaP cells via competitive binding assays (IC_{50}), dual-tracer radioligand- and fluorescence internalization studies. Biodistribution and small-animal PET imaging studies were performed in CB17-SCID and LNCaP xenograft bearing SHO mice, respectively, and complemented by intraoperative far-red fluorescence imaging using a clinical laparoscope. Additionally, fully automated serial cryosectioning and fluorescence imaging of one tumor-bearing animal as well as PSMA immunohistochemistry (IHC) and fluorescence microscopy of organ cryosections (tumor, kidney, spleen) were also performed.

Compared to the parent PSMA-I&T analogs, the PSMA-affinities of PSMA-I&F and its ^{nat}Ga-/^{nat}Lu-complexes remained high and unaffected by dye conjugation ($7.9<IC_{50}<10.5$ nM for all ligands). The same was observed for the internalization of ^{68}Ga- and ^{177}Lu-PSMA-I&F. In vivo, blood clearance of ^{68}Ga- and ^{177}Lu-PSMA-I&F was only slightly delayed by high plasma protein binding (94-95%), and very low accumulation in non-target organs was observed already at 1h p.i.. Dynamic PET imaging confirmed PSMA-specific (as demonstrated by coinjection of 2-PMPA) uptake into the LNCaP xenograft (4.5±1.8%iD/g) and the kidneys (106±23%iD/g). Tumor/background ratios of 2.1, 5.2, 9.6 and 9.6 for blood, liver, intestines and muscle, respectively, at 1h p.i. led to excellent imaging contrast in ^{68}Ga-PSMA-I&F PET and in intraoperative fluorescence imaging. Furthermore, fluorescence imaging of tissue cryosections allowed high-resolution visualization of intraorgan PSMA-I&F distribution in vivo and its correlation with PSMA expression as determined by IHC.

Downloaded from jnm.snmjournals.org by on October 29, 2018. For personal use only.

Thus, with its high PSMA-targeting efficiency and favorable pharmacokinetic profile, ^{68}Ga/^{177}Lu-PSMA-I&F serves as an excellent proof-of-concept compound for the general feasibility of PSMA-I&T-based hybrid imaging. The PSMA-I&T scaffold represents a versatile PSMA-targeted lead structure, allowing relatively straightforward adaptation to the different structural requirements of dedicated nuclear or hybrid imaging agents.

KEYWORDS

PSMA, prostate cancer, fluorescence, hybrid tracer, intraoperative guidance

Downloaded from jnm.snmjournals.org by on October 29, 2018. For personal use only.

INTRODUCTION

Triggered by the introduction of ^{68}Ga-PSMA-11 PSMA PET in 2012 (*1*) for the diagnosis and staging of prostate cancer (*2-3*), PSMA-targeted diagnostic imaging and subsequently developed therapeutic approaches (*4-6*) have become valuable new tools in the clinical management of prostate cancer (*7*).

The rapid success of this translational effort is based on the availability of powerful PSMA-targeted tracers for all relevant clinical applications (SPECT/PET/targeted radionuclide therapy) (*7-9*). Tracer development, in turn, has been facilitated by the relative tolerance of the most commonly used central PSMA binding motif, EuX (glutamate-urea-X, with X=lysine, glutamate or cysteine), towards diverse and even bulky chemical modifications (*1, 4, 10*). This allows relatively straightforward adjustment of the tracer structure to the requirements for the respective labeling strategy (^{99m}Tc, ^{18}F, diagnostic and therapeutic M^{3+} radiometals) without compromising PSMA targeting efficiency and has thus also promoted the rapid expansion of PSMA-targeted theranostics towards alpha therapy using ^{213}Bi (*11-12*) or ^{225}Ac (*13*). Furthermore, the flexibility of EuX-based tracers towards modification also supports the implementation of chemical strategies for the finetuning of their pharmacokinetic profile (*5, 14-15*) and the generation of suitable fluorescent probes (*16-18*).

Recently, the existing "classical" theranostic concept comprising diagnostic imaging and targeted radionuclide therapy has been expanded by the use of ^{111}In-PSMA-I&T (*19*) and ^{99m}Tc-PSMA-I&S (for **i**maging and **s**urgery) (*20*) for PSMA-targeted radioguided surgery of soft-tissue metastases in oligometastatic recurrent prostate cancer (*21-23*). A practical disadvantage of relying on intraoperative radioguidance alone is the acoustic and numeric surgical guidance provided by gamma probes, which, although highly sensitive, have a limited spatial resolution. As an alternative, the use of fluorescent tracers has been proposed (*24*). Although fluorescence imaging supports real-time visual image guidance, it suffers from severe attenuation in tissue and thus is not suitable to detect metastases in deeper lying lymph nodes (*25*).

Downloaded from jnm.snmjournals.org by on October 29, 2018. For personal use only.

In this context, the use of multimodal, or rather, hybrid tracers that combine gamma emission and fluorescence in one (targeted) molecule merges the best of both modalities. The unquestionable utility of such a hybrid approach has initially been established by the introduction of the hybrid sentinel lymph node tracer ICG-^{99m}Tc-nanocolloid (ICG: indocyanine green) (*26*) in different cancer types. The various prostate cancer related studies performed with this tracer have demonstrated how a hybrid tracer design can help improve radioguidance procedures (*27*), thereby triggering the recent development of various dedicated hybrid nuclear/fluorescence-probes (*28-33*).

Given the potential demonstrated by PSMA-targeted radioguided surgery, it is a logical next step to study if this procedure, similar to SLN biopsy procedures, can benefit from a hybrid fluorescent/nuclear guidance concept. First examples of PSMA-targeted hybrid tracers, either small-molecule inhibitors (*31-32*) or antibodies (*33*), have recently been evaluated preclinically and demonstrate the general feasibility of such an approach. While most tracers for fluorescence guided surgery include the commercially available near-infrared (NIR) dye IRDye800CW (λ_{ex}=773nm, λ_{em}=792nm), the far-red cyanine dye Cy5 (λ_{ex}=640nm, λ_{em}=656nm) has also been found to be of utility in surgical guidance (*34-35*). Furthermore, the superiority of Cy5 over the NIR dyes Cy7 (λ_{ex}=760nm, λ_{em}=780nm) and ICG (λ_{ex}=800nm, λ_{em}=820nm) with respect to detection sensitivity (0.05 µM vs 3.15 µM for ICG), tissue penetration (9 mm vs 6 mm for ICG) and brightness (quantum yield: 28% vs 0.3% for ICG) has recently been reported (*36*). Additionally, it was shown that the disulfonated analog of Cy5, Sulfo-Cy5 (λ_{ex}=646nm, λ_{em}=662nm), in addition to being substantially more hydrophilic, displays even more favorable characteristics with respect to optical stability and brightness ($51 \cdot 10^3$ vs $23 \cdot 10^3 \cdot M^{-1} \cdot cm^{-1}$ for Cy5) (*37*).

Sulfo-Cy5 was therefore selected as the fluorescent dye of choice for the implementation of a first-generation hybrid concept based on the PSMA-I&T scaffold (Fig. 1). Using this established backbone has the advantage of allowing an exact assessment of the influence of linker branching and dye conjugation on the pharmacokinetic properties of the novel tracer compared to the parent compounds ^{68}Ga-PSMA-

Downloaded from jnm.snmjournals.org by on October 29, 2018. For personal use only.

I&T and ^{177}Lu-PSMA-I&T, based on already existing data sets (*4*). Here, we present the in-depth preclinical evaluation of the novel hybrid analog, ^{68}Ga/^{177}Lu-PSMA-I&F (Fig. 1), with respect to PSMA-targeting efficiency and overall performance as a hybrid nuclear/fluorescent probe for the sensitive in vivo imaging of PSMA-expression. Of course, the high-energy gamma emission of ^{68}Ga-PSMA-I&F (and also of its ^{177}Lu-labeled analog) severely challenges their clinical application in radio/fluorescence guided surgery, both with respect to spatial resolution during surgery and to patient dosimetry. It is important to note, however, that PSMA-I&F was specifically designed as a first proof-of-concept compound to demonstrate the general suitability of the underlying tracer design (PSMA-I&T-based) for the generation of tailored PSMA-ligands for a broad spectrum of multimodal applications. Our previous experience with ^{99m}Tc-PSMA-I&S has demonstrated the relative ease of adapting the labeling chemistry and pharmacokinetic profile of the PSMA-I&T-scaffold to a dedicated application in radioguided surgery (*20*). Thus, a swift transfer of the insights gained in this proof-of-concept study to a next generation of corresponding ^{99m}Tc-labeled Sulfo-Cy5-PSMA-ligands with potential for a rapid transfer into the clinical/surgical setting may be anticipated.

Downloaded from jnm.snmjournals.org by on October 29, 2018. For personal use only.

MATERIALS AND METHODS

Precursor Synthesis and Radiolabeling

The synthesis of PSMA-I&F (DOTAGA-D-Lys(N_ε-Sulfo-Cy5)-D-(3-iodo)Tyr-D-(3-iodo)Tyr-D-Lys(N_ε-Sub-KuE), Fig. 1) was performed in analogy to a previously published protocol (*38*) (see supplemental data). ^{68}Ga-labeling of PSMA-I&F (5 nmol, 800 µl 2.7M HEPES) was carried out as described previously (*39*) using an automated system (GallElut$^+$ by Scintomics, Germany), and labeling with $^{177}LuCl_3$ (itm, Garching, Germany) was performed manually using a standard protocol (2 nmol precursor, 10% (v/v) 1M NH_4OAc; for details see supplemental data). The radioiodinated reference ligand (^{125}I-BA)KuE ((S)-1-carboxy-5-(4-(-^{125}I-iodo-benzamido)pentyl)-carbamoyl)-L-glutamic acid) was prepared as described (*38*).

Determination of lipophilicity and plasma protein binding

The lipophilicity of ^{68}Ga- and ^{177}Lu-PSMA-I&F was determined via a modified shake-flask method as described (*38*). Plasma protein binding of both tracers was determined using two alternative methods, i.e. incubation in fresh human plasma and subsequent ultrafiltration (*20*) and a previously established gradient HPLC method for the quantification of HSA binding (*40-41*).

In vitro evaluation

Competitive binding experiments (IC_{50}) were carried out in analogy to a previously published protocol (*38*) using LNCaP cells and (^{125}I-BA)KuE as standard radioligand. Internalization kinetics of ^{68}Ga-PSMA-I&F and ^{177}Lu-PSMA-I&F (2nM) were investigated in dual tracer internalization assays using PSMA expressing LNCaP cells and (^{125}I-BA)KuE (0.1nM) as an internal reference. For normalization, ^{68}Ga-PSMA-I&T and ^{177}Lu-PSMA-I&T (2nM) were re-assayed under these conditions. For fluorescence microscopy, PSMA-positive LNCaP and PSMA-negative PC3 cells (seeded on glass cover slips) were incubated with the respective PSMA-I&F analog (100 nM, 37°C) for 5 and 60 min, respectively, and ligand internalization was visualized using a Keyence BZ-9000 fluorescence microscope. Details are provided in the supplemental data.

Downloaded from jnm.snmjournals.org by on October 29, 2018. For personal use only.

In vivo evaluation

All animal experiments were conducted in accordance with the German Animal Welfare Act (Deutsches Tierschutzgesetz, approval no. 55.2-1-54-2532-71-13).

Biodistribution studies

The biodistribution of ^{177}Lu-PSMA-I&F was investigated in non-tumor-bearing male CB-17 SCID mice. In the case of ^{68}Ga-PSMA-I&F, biodistribution studies were carried out using LNCaP xenograft bearing SHO mice (supplemental data). Mice were injected intravenously with ^{177}Lu-PSMA-I&F (9.3 MBq) or ^{68}Ga-PSMA-I&F (13.2 MBq; the amount of injected peptide was kept constant at 0.2 nmol/mouse in all experiments) under isoflurane anaesthesia and were sacrificed at 1h (^{68}Ga-PSMA-I&F, ^{177}Lu-PSMA-I&F) and 6h (^{177}Lu-PSMA-I&F) p.i. (groups of n=5, respectively). The organs of interest were dissected, and the activity concentration in weighed tissue samples was quantified using a 2480 Automatic Gamma Counter (PerkinElmer).

PET imaging

Small animal PET imaging was performed on a Siemens Inveon small-animal PET system. Under isoflurane anesthesia, LNCaP xenograft bearing SHO mice were injected intravenously with 0.19– 0.25 nmol (2–7 MBq) of ^{68}Ga-PSMA-I&F. For competition studies, 1 µmol of 2-PMPA (2-phosphonomethyl pentanedioic acid; 226 µg/mouse) was coadministered. Dynamic imaging was performed after on-bed injection for 90 minutes. Static images were acquired 1h after tracer injection with an acquisition time of 15 minutes. Images were reconstructed as single frames using Siemens Inveon software, employing a three-dimensional ordered subset expectation maximum (OSEM3D) algorithm without scatter and attenuation correction.

Downloaded from jnm.snmjournals.org by on October 29, 2018. For personal use only.

Ex vivo fluorescence microscopy

LNCaP xenograft bearing CB-17 SCID mice were injected with 2 nmol of PSMA-I&F in 100 µl of PBS via the tail vein. At 1h p.i., mice were sacrificed, the tissues of interest were removed, embedded in Tissue-Tek (Sakura Finetek Europe B.V., Netherlands) and frozen to -18°C. Cryosections (10 µm) were prepared using a Leica CM1950 cryostat (Leica, Wetzlar, Germany), and fluorescence microscopy was performed on a Keyence BZ-9000 fluorescence microscope equipped with a Cy5 filter. Images were processed using the BZ-9000 analyzer software.

Histopathology and PSMA immunohistochemistry

Hematoxylin-Eosin staining was performed on deparaffinized 2 µm sections of mouse tissues with Eosin and Mayer's Haemalaun according to a standard protocol. Immunohistochemistry was performed using a BondMax RXm system (Leica, Wetzlar, Germany, all reagents from Leica) with a primary antibody against PSMA (abcam, Cambridge, UK, ab133579, diluted 1:100 in antibody diluent). For details see supplemental data.

Whole-body cryosectioning and fluorescence imaging

A LNCaP xenograft bearing SHO mouse (the same animal that had been used for the static PET scan two days previously) was injected with 2 nmol of ^{nat}Ga-PSMA-I&F, sacrificed at 1h p.i., embedded in a mixture of Tissue-Tek and black ink (7.41% v/v) and frozen. Whole-body cryosectioning and fluorescence imaging was performed using a Leica CM 3500 cryostat at 80 µm steps. Details on the fluorescence imaging protocol and the instrumentation are provided in the supplemental data. The serial sectioning and imaging system was fully automated, using custom software implemented in LabView (National Instruments, Austin, USA) (*42*). Post-processing was performed using MATLAB (Mathworks, Natick, USA), and Amira (FEI Visualization Sciences Group, Burlington, USA) was used for cross-sectional and longitudinal visualization of the acquired data and for three-dimensional representation of the fluorescence data.

Downloaded from jnm.snmjournals.org by on October 29, 2018. For personal use only.

Intraoperative fluorescence imaging

Fluorescence imaging (intraoperative/ex vivo) of LNCaP xenografts in CB17-SCID mice (1h p.i.) was performed using two different instrumental setups: A) a Dino-lite handheld digital microscope for Cy5 (Dino-Lite Edge AM4115T-DFRW, AnMo Electronics Corporation, Hsinchu, Taiwan) and DinoCapture 2.0 software (AnMo Electronics Corporation), and B) a 0° Firefly laparoscope that is compatible with the surgical robotic da Vinci Si system (Intuitive Surgical Inc., Sunnyvale, California, USA), using a Karl Storz fluid light cable for target illumination (495 FR; KARL STORZ Endoskope GmbH&Co.KG, Tuttlingen, Germany) and an Edmund Optics bandpass filter (Edmund Optics Inc., Barrington, NJ, USA) to isolate the Cy5 emission. Images were captured from the unprocessed Firefly video feed. For instrumental details see supplemental data.

Downloaded from jnm.snmjournals.org by on October 29, 2018. For personal use only.

RESULTS

Synthesis and Radiolabeling

PSMA-I&F was synthesized via a mixed solid phase/solution phase synthetic strategy, with coupling of Sulfo-Cy5-COOH to the fully deprotected, DOTAGA-functionalized backbone as the last step. PSMA-I&F was obtained in >96% purity (UV absorption at 214 nm) and 28% yield for dye conjugation.

Radiolabeling was carried out using standard automated (^{68}Ga) or manual (^{177}Lu) procedures, yielding ^{68}Ga-PSMA-I&F and ^{177}Lu-PSMA-I&F in isolated radiochemical yields of 74% and 98%, respectively (decay corrected). The specific activities of ^{68}Ga-PSMA-I&F and ^{177}Lu-PSMA-I&F were 61 and 55 GBq/µmol, respectively, and radiochemical purity as determined by radio-TLC was >98% for both compounds.

In vitro characterization

All in vitro data obtained for PSMA-I&F and its corresponding (radio)metal-chelates are summarized in Table 1; data for the respective PSMA-I&T reference compounds (*4*) are included for comparison. Overall, linker extension and conjugation with Sulfo-Cy5 dye lead to slightly increased lipophilicities of ^{68}Ga- and ^{177}Lu-PSMA-I&F compared to the PSMA-I&T parent compounds, resulting in stronger non-specific binding to human serum albumin. However, these structural modifications have no detectable influence on the PSMA-affinity (IC_{50}) of PSMA-I&F compared to PSMA-I&T (*4, 38*). Furthermore, and as observed for PSMA-I&T, PSMA-affinity of PSMA-I&F also remains entirely unaffected by (radio)metal chelation. The same applies to the internalization efficiency of ^{68}Ga-PSMA-I&F and ^{177}Lu-PSMA-I&F into LNCaP prostate carcinoma cells compared to ^{177}Lu-PSMA-I&T, with all three compounds showing identical tracer internalization after 1h incubation time (37°C). Only ^{68}Ga-PSMA-I&T displayed unexpectedly high internalization efficiency compared to the reference (^{125}I-BA)KuE under these conditions.

Downloaded from jnm.snmjournals.org by on October 29, 2018. For personal use only.

Fluorescence microscopy of ligand internalization

The PSMA-mediated internalization of PSMA-I&F and its ^{nat}Ga/^{nat}Lu-analogs into LNCaP cells was also investigated using fluorescence microscopy (Fig. 2). As shown exemplarily for ^{nat}Lu-PSMA-I&F in Fig. 2, ligand binding and internalization are highly PSMA-specific, since virtually no background Cy5-fluorescence was detected for the PSMA-negative PC-3 cells under the same conditions. While ^{nat}Lu-PSMA-I&F fluorescence was primarily membrane-associated after 5 min, efficient ligand internalization into the cells was observed within 60 min at 37°C. At that time point, Cy5-fluorescence was found to almost entirely co-localize with LysoTracker Green®, demonstrating rapid shuttling of ^{nat}Lu-PSMA-I&F along the endosomal pathway into the lysosomes (supplemental Fig. 2A). Furthermore, a comparative internalization assay demonstrated highly efficient and identical ligand internalization for PSMA-I&F, ^{nat}Ga-PSMA-I&F and ^{nat}Lu-PSMA-I&F, even at lower ligand concentrations (25 nM) (supplemental Fig. 2B), which is in accordance with the radioligand internalization data (Table 1).

In vivo biodistribution studies

Since the physicochemical and *in vitro* targeting characteristics of ^{68}Ga- and ^{177}Lu-PSMA-I&F were found to be nearly identical, both compounds were assumed to also display very similar *in vivo* biodistribution profiles. Due to the longer half-life of ^{177}Lu, which facilitates in vivo studies at later time points, ^{177}Lu-PSMA-I&F was selected to determine the general biodistribution and clearance kinetics of PSMA-I&F-based ligands in non tumor-bearing SCID mice at 1 and 6h p.i. (Table 2). Surprisingly, despite high plasma protein binding (Table 1), ^{177}Lu-PSMA-I&F shows relatively fast background clearance within 6h, with very low accumulation in the gastrointestinal tract and other non-target organs. However, the PSMA-mediated tracer uptake in the kidneys is high and persistent.

Although displaying a slightly higher blood concentration at 1h p.i., ^{68}Ga-PSMA-I&F shows an identical distribution pattern in almost all tissues, with the only exception of an increased renal uptake compared to ^{177}Lu-PSMA-I&F. Uptake in the LNCaP xenograft lies in the expected range (*4, 20*), leading to

Downloaded from jnm.snmjournals.org by on October 29, 2018. For personal use only.

reasonable tumor/background ratios of 2.1, 5.2, 9.6 and 9.6 for blood, liver, intestines and muscle, respectively, at 1h p.i..

Small animal PET imaging

That these target/non-target ratios are sufficient for high-contrast imaging of PSMA-expressing tumors was confirmed by ^{68}Ga-PSMA-I&F-PET (Fig. 3). Furthermore, a competition study (coinjection of an excess of 2-PMPA) demonstrated the pronounced PSMA-specificity of ^{68}Ga-PSMA-I&F uptake in tumor and kidney and blockable tracer uptake in the salivary glands. A dynamic PET scan (0-90 min p.i.) revealed fast background clearance kinetics (blood and muscle) with no indication of unwanted tracer retention as well as steadily increasing tracer accumulation in PSMA-expressing tissues (tumor, kidney) over time. Interestingly, ^{68}Ga-PSMA-I&F showed no retention in the salivary glands, but washout at a slightly slower rate than observed for muscle.

Whole-body cryosectioning and fluorescence imaging

Results from fluorescence imaging (Cy5) of single whole-body cryosections 1h after i.v. administration of ^{nat}Ga-PSMA-I&F and subsequent 3D reconstruction of the 2D data are summarized in Fig. 4. Fluorescence images show accumulation of ^{nat}Ga-PSMA-I&F in tumor, kidney and the salivary glands with relative fluorescence intensities that correlate closely with the respective tracer uptake observed in the PET imaging studies using ^{68}Ga-PSMA-I&F (Fig. 3). Additionally, due to its superior spatial resolution and sensitivity, which surpasses that of nuclear imaging techniques by orders of magnitude, fluorescence imaging reveals considerable inhomogeneity of ^{nat}Ga-PSMA-I&F uptake in the tumor xenograft as well as the restriction of renal ^{nat}Ga-PSMA-I&F uptake to the kidney cortex. Furthermore, homogenous accumulation in the salivary glands (Figs. 4, A and B) and faint, but discernible ligand uptake in PSMA-positive thoracic paravertebral ganglia, that has also been documented in humans (*43-45*), were observed (Fig. 4A).

Downloaded from jnm.snmjournals.org by on October 29, 2018. For personal use only.

Immunohistochemistry and fluorescence microscopy

To investigate the dependence of PSMA-I&F uptake in different mouse organs (tumor, kidney, spleen) on *in vivo* PSMA expression, PSMA immunohistochemistry was performed on tissue samples of LNCaP xenograft bearing CB-17 SCID mice, and immunohistochemistry data were compared to the results obtained by fluorescence microscopy of tissue cryosections 1h p.i. of PSMA-I&F in the same tumor model (Fig. 5).

PSMA immunohistochemistry revealed intense and homogenous membrane staining of all tumor cells in the LNCaP tumor xenograft, whereas spleen tissue was found to be essentially PSMA negative. Only very weak membranous staining of single vascular endothelial cells as well as single lymphocytes within the red pulp of the spleen was observed. In kidney, intense PSMA staining was detected in parietal cells of the Bowman capsule and the proximal convoluted tubules (luminal membrane), alongside with gradually decreasing PSMA expression in the more distal parts of the renal tubules. The same distribution pattern with moderate to high locally restricted uptake of PSMA-I&F in the renal cortex was observed in fluorescence microscopy, indicating PSMA-specific accumulation in the tubules and glomeruli. However, in contradiction to the virtually non-existent PSMA expression in spleen, fluorescence microscopy reveals homogenous membrane binding of PSMA-I&F to spleen tissue. Also in tumor, PSMA-I&F uptake does not consistently correlate with the immunohistochemistry data. While PSMA expression is very high throughout the entire tumor specimen, accumulation of PSMA-I&F is inhomogeneous. In contrast to spleen, however, PSMA-I&F fluorescence is not only membrane-associated but also seems to be internalized into tumor cells, as suggested by high cytosolic ligand uptake.

Fluorescence guided surgery

To demonstrate the suitability of PSMA-I&F as a targeted probe for the intraoperative detection and fluorescence guided resection of PSMA expressing prostate carcinoma tissue, and to investigate the general compatibility of a Cy5-conjugated fluorescent probe with clinically used fluorescence cameras

Downloaded from jnm.snmjournals.org by on October 29, 2018. For personal use only.

such as the Firefly laparoscope, proof-of-concept intraoperative and ex vivo fluorescence imaging using PSMA-I&F was performed in a LNCaP tumor bearing mouse (Fig. 6). Both experimental settings allowed the sensitive in vivo detection of the PSMA-I&F positive tumor xenograft with good contrast to the surrounding tissue.

DISCUSSION

The results obtained in the preclinical evaluation of the novel PSMA-targeted hybrid compound, ^{68}Ga/^{177}Lu-PSMA-I&F, supply convincing evidence for the validity of the major working hypothesis, on which the design of this proof-of-concept compound was based, i.e. that the PSMA-I&T scaffold is a versatile PSMA-targeted molecular platform for the generation of structurally diverse nuclear and hybrid probes.

This is primarily supported by two findings: the nearly identical PSMA-targeting efficiency observed for PSMA-I&F and its ^{68}Ga- and ^{177}Lu-labeled analogs compared to the respective PSMA-I&T reference compounds (Fig. 1, Table 1), both in vitro and in vivo, and the comparably small effect of linker extension and dye conjugation on the pharmacokinetics and in vivo performance of PSMA-I&F.

In contrast, for other structurally similar hybrid PSMA inhibitors such as ^{111}In-DOTA-Lys(N_ε-IRDye800CW)-Sub-KuE (*31*) or IRDye800CW-^{68}Ga-HBED-CC-KuE (*32*), both dye conjugation and metal chelation were found to have considerable impact on PSMA affinity and/or internalization efficiency as well as in vivo biodistribution and clearance kinetics. While for ^{111}In-DOTA-Lys(N_ε-IRDye800CW)-Sub-KuE, PSMA-affinity was found to remain essentially unaffected by dye conjugation (*10, 31*), its background clearance was substantially delayed compared to the parent compound ^{68}Ga-DOTA-Lys-Sub-KuE (*10*), as indicated by a 5-fold increased blood activity concentration at 1h p.i.. Consequently, tracer uptake in the excretion organs and the tumor xenograft (PC-3 PIP) were also increased by a factor of 2-4.

In the case of the fluorescently labeled ^{68}Ga-HBED-CC-KuE analogs (*32*), conjugation with NIR dyes lead to a loss in PSMA-affinity, but also an unexpected increase in internalization efficiency. Again, tracer

Downloaded from jnm.snmjournals.org by on October 29, 2018. For personal use only.

clearance from the circulation and from the background was markedly delayed, but accumulation in the LNCaP tumors was also threefold increased.

These effects were not observed for ^{68}Ga-PSMA-I&F. In our study, attachment of Sulfo-Cy5 conveys a slight increase in lipophilicity and plasma protein binding (Tab. 1), leading to slightly delayed clearance kinetics of ^{68}Ga-PSMA-I&F compared to ^{68}Ga-PSMA-I&T. Only a negligible effect on tracer accumulation in the excretion organs is observed (Tab. 2), ultimately providing interchangeable PET imaging results using ^{68}Ga-PSMA-I&F (Fig. 3) and ^{68}Ga-PSMA-I&T (*4*).

Interestingly, although the observed effects of the respective fluorescent dye on PSMA-targeting, clearance kinetics and the biodistribution pattern of ^{111}In-DOTA-Lys(N_ε-IRDye800CW)-Sub-KuE, IRDye800CW-^{68}Ga-HBED-CC-KuE and ^{68}Ga-PSMA-I&F are fundamentally different, the tumor/background ratios for the three compounds are very similar (t/blood, t/liver, t/intestines and t/muscle: 1.4, 5.8, 7.7 and 11.6 (^{111}In-DOTA-Lys(N_ε-IRDye800CW)-Sub-KuE (*31*)), 4.5, 4.9, 5.7 and 4.8 (IRDye800CW-^{68}Ga-HBED-CC-KuE (*32*)) and 2.1, 5.2, 9.6 and 9.6 (^{68}Ga-PSMA-I&F), respectively).

Overall, however, using the PSMA-I&T scaffold in combination with the comparably small Sulfo-Cy5 dye has the distinct advantage of providing PSMA-I&F as a hybrid probe with reliable PSMA-targeting properties and a suitable biodistribution pattern. Additionally, the general utility of the far-red dye Sulfo-Cy5 for sensitive ex vivo and in vivo fluorescence imaging is supported by the imaging data obtained with PSMA-I&F (Figs. 4, 5 and 6). Particularly noteworthy in this context is the compatibility of Sulfo-Cy5 with not only dedicated preclinical fluorescence cameras, but also with the clinical Firefly laparoscope (Fig. 6), which was able to detect the PSMA-I&F accumulating LNCaP xenograft with high sensitivity. With world-wide > 4000 installs of surgical robots equipped with this camera (Source: Intuitive Surgical Inc.), the general translational potential of Sulfo-Cy5-conjugated targeted hybrid probes for intraoperative guidance is thus greatly enhanced.

Downloaded from jnm.snmjournals.org by on October 29, 2018. For personal use only.

A relatively surprising result from our fluorescence microscopy studies (Fig. 5) that is worth mentioning is the limited accordance of PSMA-I&F accumulation in tumor, kidney and spleen with the corresponding PSMA-expression level. Only in kidney, excellent co-localization of focal tubular PSMA-expression and PSMA-I&F uptake was detected. These data accurately reflect the human situation, where endogenous tubular PSMA expression (*46*) is primarily held responsible for the generally high renal uptake of PSMA-targeted radiotracers. However, given the comparably low overall renal PSMA-expression compared to tumor (Fig. 5), the observed >20-fold higher (and only partly blockable (Fig. 3)) uptake of ^{68}Ga-PSMA-I&F in kidney compared to the LNCaP xenograft is strongly indicative of alternative, non-PSMA-mediated uptake mechanisms such as megalin/cubilin mediated tubular reabsorption (*47*) being involved in the renal handling of PSMA-targeted tracers.

In tumor, tracer uptake was substantially lower and less homogenous that what would have been expected from the consistently very high PSMA-expression throughout the entire specimen. Here, limited perfusion of the fast-growing xenograft seems the most probable reason for the observed inhomogeneous PSMA-I&F uptake.

For spleen, the most contradictory results were obtained. The observed absence of PSMA expression in mouse spleen is in agreement with data from the literature, reporting PSMA expression in mouse spleen on the mRNA-level (*48*), but not on the protein level (*49*). However, homogenous membrane binding of PSMA-I&F was observed, resulting in the observed high uptake of ^{68}Ga-PSMA-I&F in the spleen (Table 2). Thus, although being efficiently blockable by an excess of 2-PMPA (*20*), the splenic uptake of PSMA-I&T based ligands in mice seems to be mediated by a PSMA-independent process, and further studies, also with respect to the significance of these observations for the human situation, are required.

CONCLUSION

The preclinical evaluation of PSMA-I&F and its ^{68}Ga- and ^{177}Lu-labeled analogs has conclusively demonstrated the general feasibility of a PSMA-I&T-based hybrid tracer concept using the far-red

Downloaded from jnm.snmjournals.org by on October 29, 2018. For personal use only.

fluorescent dye Sulfo-Cy5. Despite substantial structural changes compared to the parent compound ^{68}Ga/^{177}Lu-PSMA-I&T, ^{68}Ga/^{177}Lu-PSMA-I&F maintains an unchanged, high PSMA-targeting efficiency and a favorable pharmacokinetic profile, allowing for sensitive and high-contrast detection of PSMA-expression in vivo via nuclear (PET/SPECT) and optical imaging methods (intraoperative imaging/in vivo and ex vivo fluorescence microscopy). Thus, the PSMA-I&T scaffold has once more been shown to represent a versatile PSMA-targeted molecular platform, which allows relatively straightforward adaptation to the different structural requirements of dedicated nuclear or hybrid imaging agents.

DISCLOSURE STATEMENT

This study was financially supported by the Deutsche Forschungsgemeinschaft (SFB824; subproject Z1). Hans-Jürgen Wester is founder and shareholder of Scintomics GmbH. Vasilis Ntziachristos serves as consultant for SurgVision BV, and Maximilian Koch is an employee of Bracco Imaging Germany GmbH. No other potential conflict of interest relevant to this article was reported.

ACKNOWLEDGMENTS

The authors thank Sven Hintze and Sarah Glasl for their excellent technical support. We are also indebted to Sybille Reder and Markus Mittelhäuser for their valuable contribution with respect to small animal PET imaging. Material support for this work was provided by Intuitive Surgical (Intuitive Surgical Inc., Sunnyvale, California), supplying the authors with a stand-alone Firefly fluorescence laparoscope system for laboratory experiments.

Downloaded from jnm.snmjournals.org by on October 29, 2018. For personal use only.

REFERENCES

1. Eder M, Schafer M, Bauder-Wust U, et al. ^{68}Ga-complex lipophilicity and the targeting property of a urea-based PSMA inhibitor for PET imaging. *Bioconjug Chem.* 2012;23:688-697.
2. Afshar-Oromieh A, Holland-Letz T, Giesel FL, et al. Diagnostic performance of ^{68}Ga-PSMA-11 (HBED-CC) PET/CT in patients with recurrent prostate cancer: evaluation in 1007 patients. *Eur J Nucl Med Mol Imaging.* 2017;44:1258-1268.
3. Rauscher I, Duwel C, Haller B, et al. Efficacy, Predictive Factors, and Prediction Nomograms for ^{68}Ga-labeled Prostate-specific Membrane Antigen-ligand Positron-emission Tomography/Computed Tomography in Early Biochemical Recurrent Prostate Cancer After Radical Prostatectomy. *Eur Urol.* 2018;73:656-661.
4. Weineisen M, Schottelius M, Simecek J, et al. Ga-68- and Lu-177-Labeled PSMA I&T: Optimization of a PSMA-Targeted Theranostic Concept and First Proof-of-Concept Human Studies. *J Nucl Med.* 2015;56:1169-1176.
5. Benesova M, Schafer M, Bauder-Wust U, et al. Preclinical Evaluation of a Tailor-Made DOTA-Conjugated PSMA Inhibitor with Optimized Linker Moiety for Imaging and Endoradiotherapy of Prostate Cancer. *J Nucl Med.* 2015;56:914-920.
6. Heck MM, Retz M, Tauber R, Knorr K, Kratochwil C, Eiber M. PSMA-targeted radioligand therapy in prostate cancer. *Urologe A.* 2017;56:32-39.
7. Virgolini I, Decristoforo C, Haug A, Fanti S, Uprimny C. Current status of theranostics in prostate cancer. *Eur J Nucl Med Mol Imaging.* 2018;45:471-495.
8. Eiber M, Fendler WP, Rowe SP, et al. Prostate-Specific Membrane Antigen Ligands for Imaging and Therapy. *J Nucl Med.* 2017;58:67S-76S.
9. Lutje S, Heskamp S, Cornelissen AS, et al. PSMA Ligands for Radionuclide Imaging and Therapy of Prostate Cancer: Clinical Status. *Theranostics.* 2015;5:1388-1401.
10. Banerjee SR, Pullambhatla M, Byun Y, et al. ^{68}Ga-labeled inhibitors of prostate-specific membrane antigen (PSMA) for imaging prostate cancer. *J Med Chem.* 2010;53:5333-5341.
11. Nonnekens J, Chatalic KL, Molkenboer-Kuenen JD, et al. ^{213}Bi-Labeled Prostate-Specific Membrane Antigen-Targeting Agents Induce DNA Double-Strand Breaks in Prostate Cancer Xenografts. *Cancer Biother Radiopharm.* 2017;32:67-73.
12. Sathekge M, Knoesen O, Meckel M, Modiselle M, Vorster M, Marx S. ^{213}Bi-PSMA-617 targeted alpha-radionuclide therapy in metastatic castration-resistant prostate cancer. *Eur J Nucl Med Mol Imaging.* 2017;44:1099-1100.
13. Kratochwil C, Bruchertseifer F, Giesel FL, et al. ^{225}Ac-PSMA-617 for PSMA-Targeted alpha-Radiation Therapy of Metastatic Castration-Resistant Prostate Cancer. *J Nucl Med.* 2016;57:1941-1944.
14. Lutje S, Slavik R, Fendler W, Herrmann K, Eiber M. PSMA ligands in prostate cancer - Probe optimization and theranostic applications. *Methods.* 2017;130:42-50.
15. Benesova M, Umbricht CA, Schibli R, Muller C. Albumin-Binding PSMA Ligands: Optimization of the Tissue Distribution Profile. *Mol Pharm.* 2018;15:934-946.
16. Chen Y, Pullambhatla M, Banerjee SR, et al. Synthesis and biological evaluation of low molecular weight fluorescent imaging agents for the prostate-specific membrane antigen. *Bioconjug Chem.* 2012;23:2377-2385.
17. Bao K, Lee JH, Kang H, Park GK, El Fakhri G, Choi HS. PSMA-targeted contrast agents for intraoperative imaging of prostate cancer. *Chem Commun (Camb).* 2017;53:1611-1614.
18. Wang X, Huang SS, Heston WD, Guo H, Wang BC, Basilion JP. Development of targeted near-infrared imaging agents for prostate cancer. *Mol Cancer Ther.* 2014;13:2595-2606.
19. Schottelius M, Wirtz M, Eiber M, Maurer T, Wester HJ. [(111)In]PSMA-I&T: expanding the spectrum of PSMA-I&T applications towards SPECT and radioguided surgery. *EJNMMI research.* 2015;5:68.

Downloaded from jnm.snmjournals.org by on October 29, 2018. For personal use only.

20. Robu S, Schottelius M, Eiber M, et al. Preclinical Evaluation and First Patient Application of ^{99m}Tc-PSMA-I&S for SPECT Imaging and Radioguided Surgery in Prostate Cancer. *J Nucl Med.* 2017;58:235-242.
21. Maurer T, Schwamborn K, Schottelius M, et al. PSMA Theranostics Using PET and Subsequent Radioguided Surgery in Recurrent Prostate Cancer. *Clin Genitourin Cancer.* 2016;14:e549-e552.
22. Rauscher I, Duwel C, Wirtz M, et al. Value of ^{111}In-prostate-specific membrane antigen (PSMA)-radioguided surgery for salvage lymphadenectomy in recurrent prostate cancer: correlation with histopathology and clinical follow-up. *BJU Int.* 2017;120:40-47.
23. Rauscher I, Horn T, Eiber M, Gschwend JE, Maurer T. Novel technology of molecular radio-guidance for lymph node dissection in recurrent prostate cancer by PSMA-ligands. *World J Urol.* 2018.
24. Neuman BP, Eifler JB, Castanares M, et al. Real-time, near-infrared fluorescence imaging with an optimized dye/light source/camera combination for surgical guidance of prostate cancer. *Clin Cancer Res.* 2015;21:771-780.
25. van Leeuwen FW, van der Poel HG. Surgical Guidance in Prostate Cancer: "From Molecule to Man" Translations. *Clin Cancer Res.* 2016;22:1304-1306.
26. Brouwer OR, Buckle T, Vermeeren L, et al. Comparing the hybrid fluorescent-radioactive tracer indocyanine green-^{99m}Tc-nanocolloid with ^{99m}Tc-nanocolloid for sentinel node identification: a validation study using lymphoscintigraphy and SPECT/CT. *J Nucl Med.* 2012;53:1034-1040.
27. KleinJan GH, van den Berg NS, de Jong J, et al. Multimodal hybrid imaging agents for sentinel node mapping as a means to (re)connect nuclear medicine to advances made in robot-assisted surgery. *Eur J Nucl Med Mol Imaging.* 2016;43:1278-1287.
28. Bugby SL, Lees JE, Perkins AC. Hybrid intraoperative imaging techniques in radioguided surgery: present clinical applications and future outlook. *Clin Transl Imaging.* 2017;5:323-341.
29. Gambini JP, Quinn TP. Hybrid tracers and devices for intraoperative imaging: the future for radioguided surgery ? *Clin Transl Imaging.* 2016;4:343-351.
30. Lutje S, Rijpkema M, Helfrich W, Oyen WJ, Boerman OC. Targeted radionuclide and fluorescence dual-modality imaging of cancer: preclinical advances and clinical translation. *Mol Imaging Biol.* 2014;16:747-755.
31. Banerjee SR, Pullambhatla M, Byun Y, et al. Sequential SPECT and optical imaging of experimental models of prostate cancer with a dual modality inhibitor of the prostate-specific membrane antigen. *Angew Chem Int Ed Engl.* 2011;50:9167-9170.
32. Baranski AC, Schafer M, Bauder-Wust U, et al. PSMA-11 Derived Dual-labeled PSMA-Inhibitors for Preoperative PET Imaging and Precise Fluorescence-Guided Surgery of Prostate Cancer. *J Nucl Med.* 2017.
33. Lutje S, Rijpkema M, Franssen GM, et al. Dual-Modality Image-Guided Surgery of Prostate Cancer with a Radiolabeled Fluorescent Anti-PSMA Monoclonal Antibody. *J Nucl Med.* 2014;55:995-1001.
34. Burggraaf J, Kamerling IM, Gordon PB, et al. Detection of colorectal polyps in humans using an intravenously administered fluorescent peptide targeted against c-Met. *Nat Med.* 2015;21:955-961.
35. Buckle T, van Willigen DM, Spa SJ, et al. Tracers for fluorescence-guided surgery: how elongation of the polymethine chain in cyanine dyes alters the pharmacokinetics of a (bimodal) c[RGDyK] tracer. *J Nucl Med.* 2018;59:986-992.
36. van Willigen DM, van den Berg NS, Buckle T, et al. Multispectral fluorescence guided surgery; a feasibility study in a phantom using a clinical-grade laparoscopic camera system. *Am J Nucl Med Mol Imaging.* 2017;7:138-147.
37. Spa SJ, Hensbergen AW, van der Wal S, Kuil J, Van Leeuwen FW. The influence of systematic structure alterations on the photophysical properties and conjugation characteristics of asymmetric cyanine 5 dyes. *Dyes and Pigments.* 2018;in press.
38. Weineisen M, Simecek J, Schottelius M, Schwaiger M, Wester HJ. Synthesis and preclinical evaluation of DOTAGA-conjugated PSMA ligands for functional imaging and endoradiotherapy of prostate cancer. *EJNMMI research.* 2014;4:63.

Downloaded from jnm.snmjournals.org by on October 29, 2018. For personal use only.

39. Notni J, Simecek J, Hermann P, Wester HJ. TRAP, a powerful and versatile framework for gallium-68 radiopharmaceuticals. *Chemistry.* 2011;17:14718-14722.
40. Valko K, Nunhuck S, Bevan C, Abraham MH, Reynolds DP. Fast gradient HPLC method to determine compounds binding to human serum albumin. Relationships with octanol/water and immobilized artificial membrane lipophilicity. *J Pharm Sci.* 2003;92:2236-2248.
41. Schottelius M, Osl T, Poschenrieder A, et al. [^{177}Lu]pentixather: Comprehensive Preclinical Characterization of a First CXCR4-directed Endoradiotherapeutic Agent. *Theranostics.* 2017;7:2350-2362.
42. Symvoulidis P, Perez CC, Schwaiger M, Ntziachristos V, Westmeyer GG, Serial sectioning and multispectral imaging system for versatile biomedical applications. In *2014 IEEE 11th International Symposium on Biomedical Imaging (ISBI)*, 2014;890-893.
43. Kanthan GL, Hsiao E, Vu D, Schembri GP. Uptake in sympathetic ganglia on ^{68}Ga-PSMA-HBED PET/CT: A potential pitfall in scan interpretation. *J Med Imaging Radiat Oncol.* 2017;61:732-738.
44. Rischpler C, Beck TI, Okamoto S, et al. ^{68}Ga-PSMA-HBED-CC uptake in cervical, coeliac and sacral ganglia as an important pitfall in prostate cancer PET imaging. *J Nucl Med.* 2018.
45. Werner RA, Sheikhbahaei S, Jones KM, et al. Patterns of uptake of prostate-specific membrane antigen (PSMA)-targeted ^{18}F-DCFPyL in peripheral ganglia. *Ann Nucl Med.* 2017;31:696-702.
46. Silver DA, Pellicer I, Fair WR, Heston WD, Cordon-Cardo C. Prostate-specific membrane antigen expression in normal and malignant human tissues. *Clin Cancer Res.* 1997;3:81-85.
47. Vegt E, Melis M, Eek A, et al. Renal uptake of different radiolabelled peptides is mediated by megalin: SPECT and biodistribution studies in megalin-deficient mice. *Eur J Nucl Med Mol Imaging.* 2011;38:623-632.
48. Hlouchova K, Navratil V, Tykvart J, Sacha P, Konvalinka J. GCPII variants, paralogs and orthologs. *Curr Med Chem.* 2012;19:1316-1322.
49. Bacich DJ, Pinto JT, Tong WP, Heston WD. Cloning, expression, genomic localization, and enzymatic activities of the mouse homolog of prostate-specific membrane antigen/NAALADase/folate hydrolase. *Mamm Genome.* 2001;12:117-123.

Downloaded from jnm.snmjournals.org by on October 29, 2018. For personal use only.

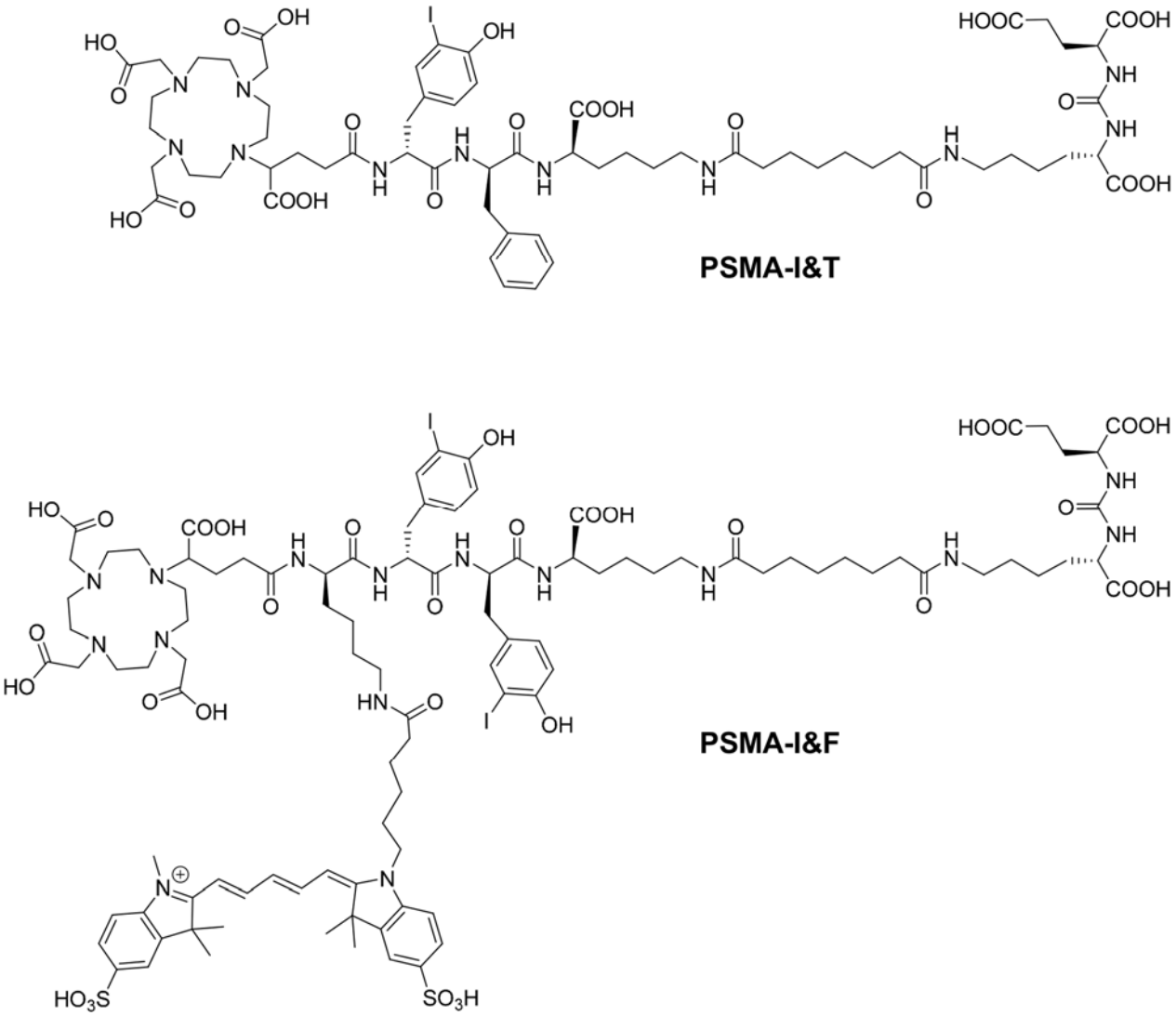

Figure 1 *Structure of PSMA-I&T (4) and its Sulfo-Cy5 conjugated hybrid analog, PSMA-I&F*

Downloaded from jnm.snmjournals.org by on October 29, 2018. For personal use only.

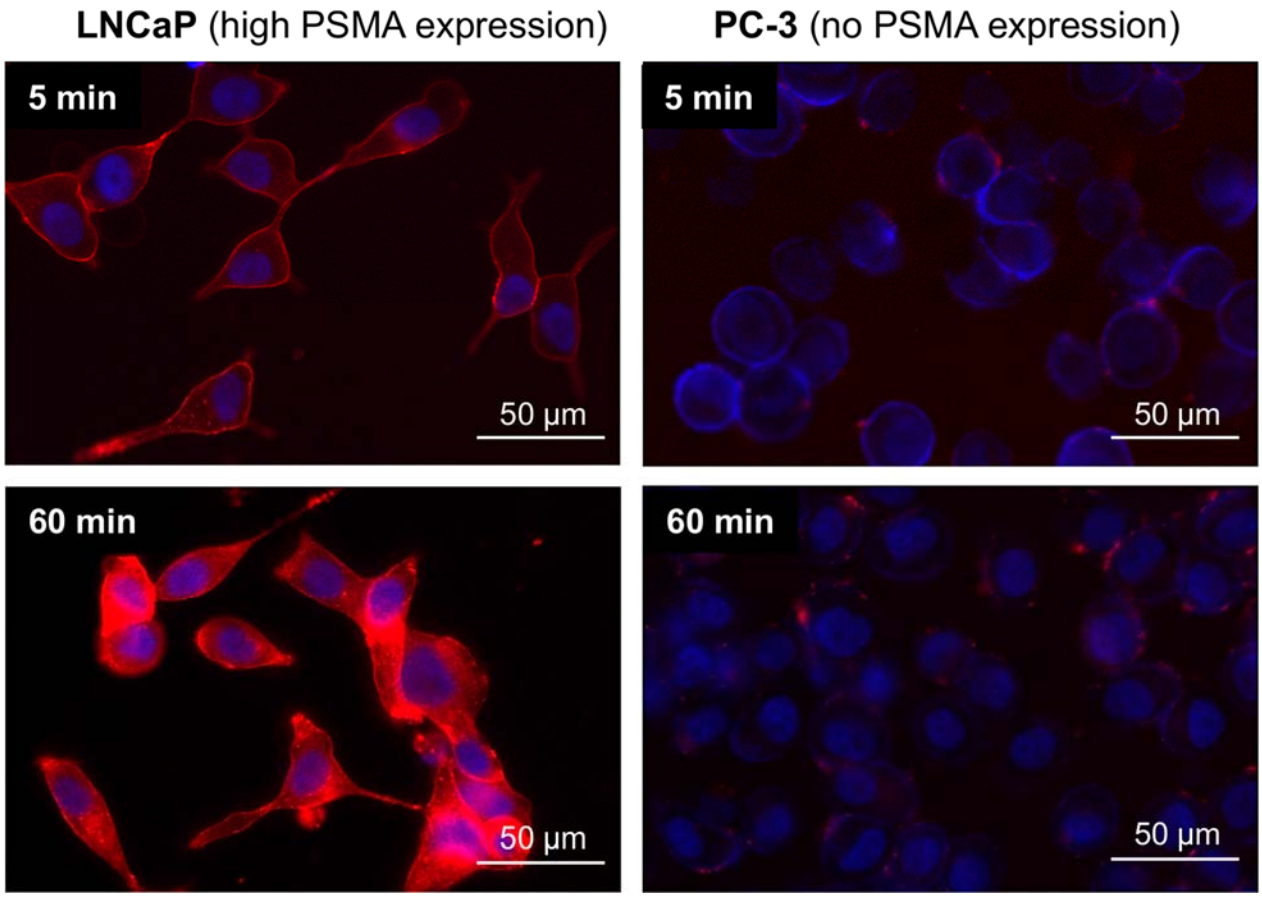

Figure 2 *Fluorescence microscopy (overlay) of the internalization of [^{nat}Lu]PSMA-I&F (100 nM) into LNCaP prostate carcinoma cells after 5 (left upper panel) and 60 (left lower panel) min at 37°C. Non-specific background internalization was determined using PSMA negative PC-3 cells (right panels). Red fluorescence: Cy5 filter (PSMA-I&F), blue fluorescence: DAPI filter (Hoechst 33342).*

Downloaded from jnm.snmjournals.org by on October 29, 2018. For personal use only.

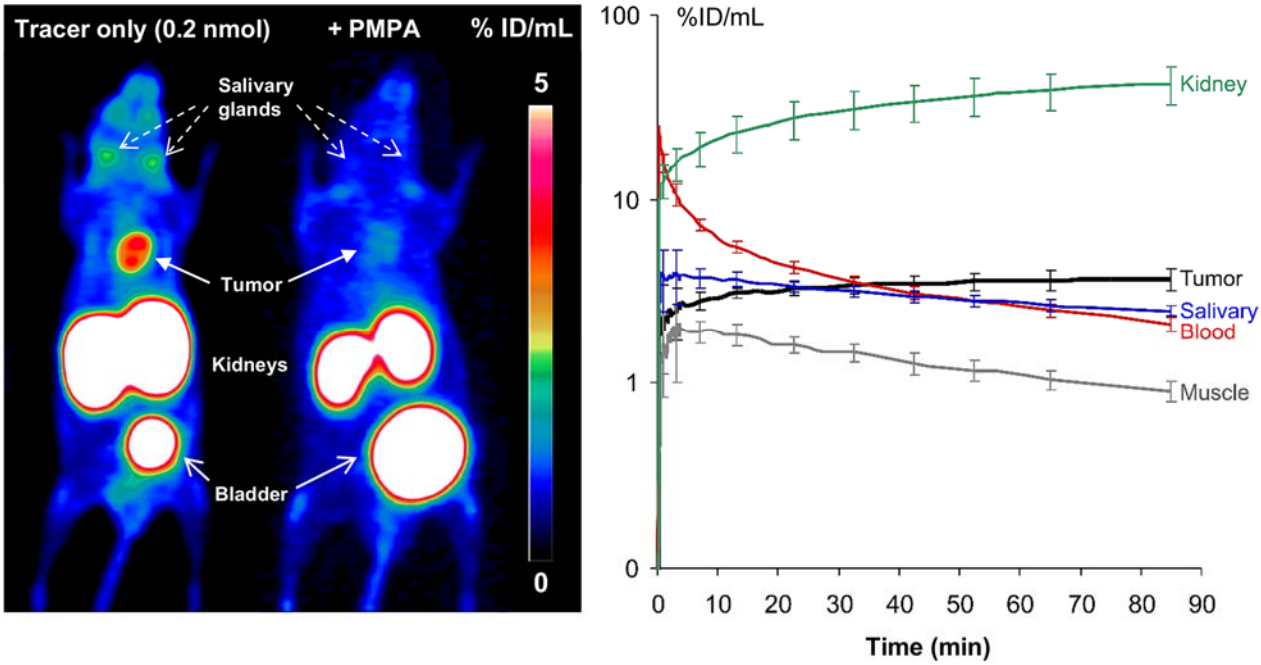

Figure 3 ***left panel*** *^{68}Ga-PSMA-I&F-PET of LNCaP xenograft bearing SHO mice (MIP, static scan, 1h p.i.) without (left mouse) or with (right mouse) coinjection of excess 2-PMPA.*

right panel *Time activity curves for selected organs 0-90min p.i. of ^{68}Ga-PSMA-I&F (0.2 nmol) in a LNCaP xenograft bearing SHO mouse.*

Downloaded from jnm.snmjournals.org by on October 29, 2018. For personal use only.

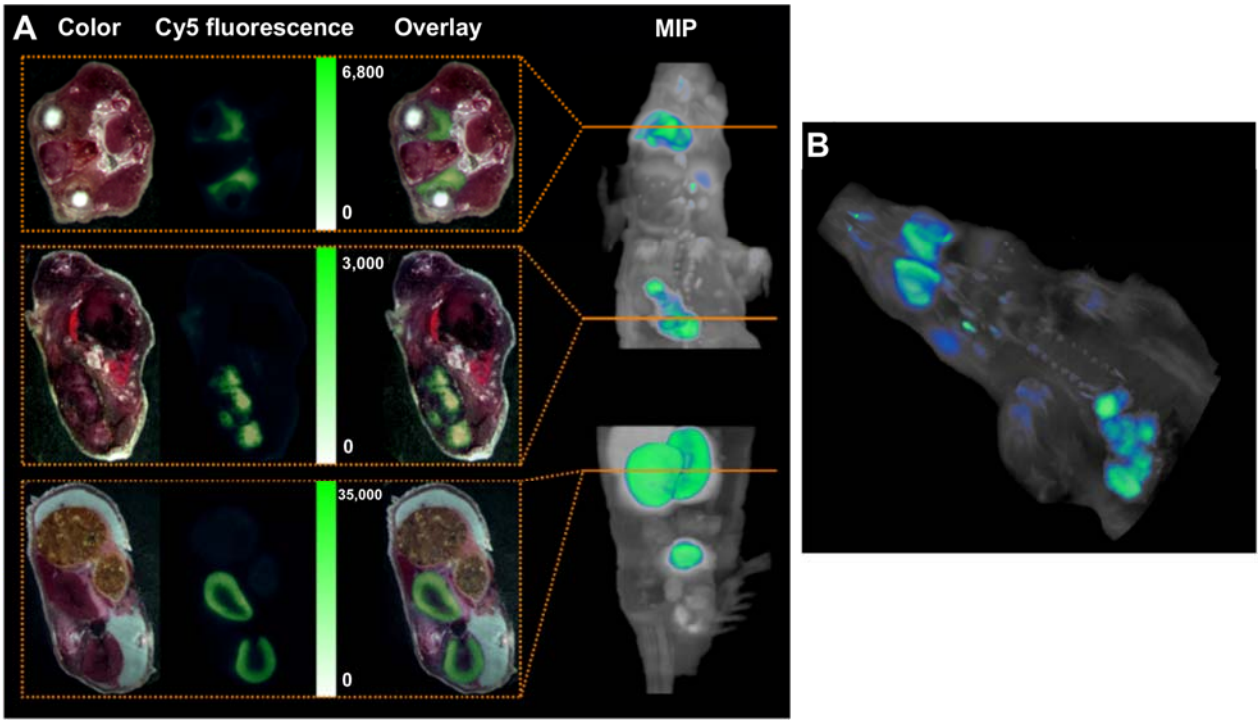

Figure 4 ***A:*** *Color and fluorescence images of whole-body cryosections of a LNCaP xenograft bearing SHO mouse 1h p.i. of 2 nmol ^{nat}Ga-PSMA-I&F. Upper row: representative section of the salivary glands, middle row: representative section of the tumor region, lower row: representative section of the kidneys. Please note that images are scaled to the same visual intensity. On the right the maximum intensity projection (MIP) at the xz plane. The orange lines correspond to the exact locations of the representative sections shown to the left.*

B*: 3D-rendering of Sulfo-Cy5 fluorescence images obtained for consecutive 2D whole-body cryosections (as in B) of a LNCaP xenograft bearing SHO mouse 1h p.i. of 2 nmol ^{nat}Ga-PSMA-I&F.*

Downloaded from jnm.snmjournals.org by on October 29, 2018. For personal use only.

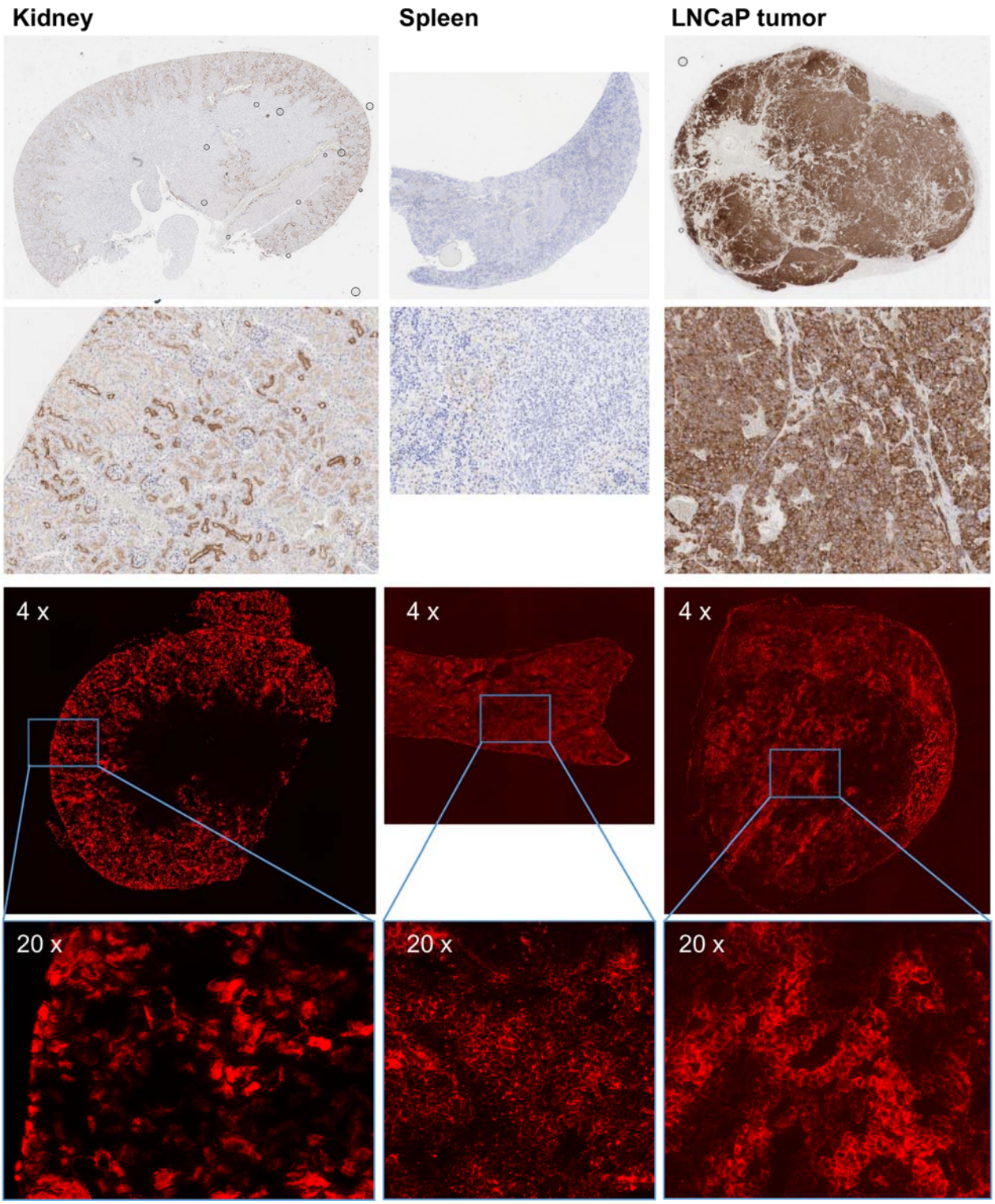

Figure 5 *Upper two rows: PSMA immunohistochemistry of mouse tissue sections (paraffin embedded, 2 µm); first row: whole organ; second row: kidney and tumor 10x, spleen 20x magnification.*
Lower two rows: Tissue distribution of PSMA-I&F (2 nmol, 1h p.i.) observed by Sulfo-Cy5 fluorescence microscopy of mouse tissue cryosections (10 µm). Third row: 4-fold magnification, fourth row: 20-fold magnification. Please note that Images have been scaled to a comparable visual fluorescence intensity. Exposition times during fluorescence microscopy: 2s for kidney, 12s for spleen and tumor, respectively.

Downloaded from jnm.snmjournals.org by on October 29, 2018. For personal use only.

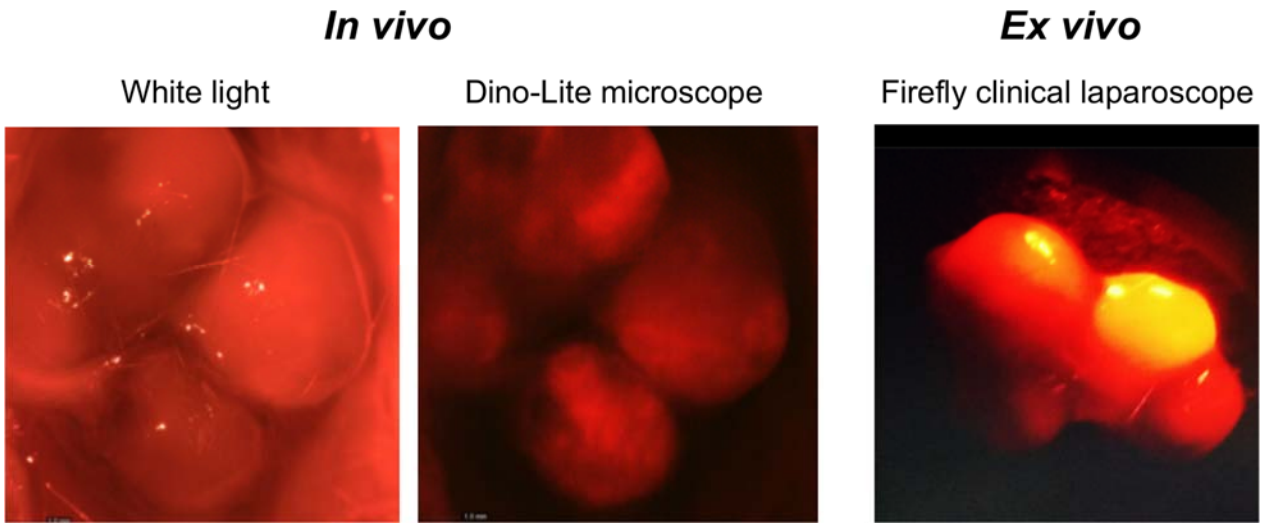

Figure 6 *Left panel: White light visualization and in vivo intraoperative fluorescence imaging of the tumor in an LNCaP xenograft bearing CB-17 SCID mouse 1h p.i. of 2 nmol PSMA-I&F. Sulfo-Cy5 fluorescence was detected using a hand-held Dino-Lite digital microscope.*
Right panel: ex vivo Sulfo-Cy5 fluorescence imaging of the same (excised) LNCaP tumor using a clinical Firefly laparoscope.

Downloaded from jnm.snmjournals.org by on October 29, 2018. For personal use only.

Table 1 *PSMA affinities, internalization and lipophilicity of Ga- and Lu-PSMA-I&T (4) and of the respective unlabeled and labeled PSMA-I&F analogs.*

Ligand	**IC_{50}** (nM)		**Specific internalization** (% of reference)*	**Lipophilicity** (log P_{OW})	**Plasma Protein Binding** (%)§
PSMA-I&T	10.2±3.5				
Ga-PSMA-I&T	9.3±3.3	^{68}Ga-PSMA-I&T	206±16	-4.30	52.0 (84.2)
Lu-PSMA-I&T	7.9±2.4	^{177}Lu-PSMA-I&T	114±8	-4.12	78.6 (82.1)
PSMA-I&F	10.3±0.7				98.3
Ga-PSMA-I&F	10.5±2.1	^{68}Ga-PSMA-I&F	103±9	-3.40	93.7 (94.0)
Lu-PSMA-I&F	9.6±1.7	^{177}Lu-PSMA-I&F	106±2	-3.53	95.0 (98.9)

* Specific internalization (total internalization corrected by internalization in the presence of 10 µM 2-PMPA) of the reference compound ([^{125}I]IBA)KuE was determined in the same experiment (dual tracer study) and used for data normalization. Data represent specific internalization at 1h incubation time.

§ Numbers represent HSA binding of the non-radioactive compounds determined via chromatography; numbers in paren-theses represent plasma protein binding determined using fresh human plasma and the corresponding radiolabeled analogs

Downloaded from jnm.snmjournals.org by on October 29, 2018. For personal use only.

Table 2 *Biodistribution of ^{177}Lu-PSMA-I&F and ^{68}Ga-PSMA-I&F in CB-17 SCID and LNCaP xenograft bearing SHO mice, respectively (n=4-5). Data are given in %iD/g and are means±SD. Data for ^{68}Ga-PSMA-I&T from a previous publication (4) are included for comparison.*

organ	[^{177}Lu]PSMA-I&F		68Ga-PSMA-I&F	68Ga-PSMA-I&T
	1h p.i.	*6h p.i.*	*1h p.i.*	*1 h p.i.*
blood	1.4±0.2	0.29±0.03	2.1±0.4	0.5±0.2
heart	0.8±0.1	0.24±0.04	1.0±0.1	0.3±0.1
lung	2.0±0.3	0.81±0.18	2.1±0.5	1.5±0.4
liver	1.4±0.5	0.58±0.08	0.9±0.1	1.0±0.4
spleen	14.6±3.9	5.71±0.60	12.8±6.5	3.9±1.5
pancreas	0.8±0.2	0.23±0.04	0.7±0.1	0.5±0.2
stomach	0.6±0.1	0.28±0.06	0.7±0.1	0.4±0.1
intestines	0.4±0.1	0.29±0.10	0.5±0.2	0.3±0.1
kidneys	76.9±4.2	72.62±5.88	105.8±22.7	53.3±9.0
muscle	0.4±0.1	0.11±0.03	0.5±0.1	0.4±0.1
LNCaP tumor	-	-	4.5±1.8	4.9±1.6

Downloaded from jnm.snmjournals.org by on October 29, 2018. For personal use only.

Supplemental data

to

Synthesis and preclinical characterization of the PSMA-targeted hybrid tracer PSMA-I&F for nuclear and fluorescence imaging of prostate cancer

Margret Schottelius*[1], Alexander Wurzer[1], Katharina Wissmiller[1], Roswitha Beck[1], Maximilian Koch[2], Dimitris Gorpas[2], Johannes Notni[1], Tessa Buckle[3], Matthias N. van Oosterom[3], Katja Steiger[4], Vasilis Ntziachristos[2], Markus Schwaiger[5], Fijs W.B. van Leeuwen[3], Hans-Jürgen Wester[1]

[1] Chair for Pharmaceutical Radiochemistry, Technische Universität München, Walther-Meissner-Strasse 3, 85748 Garching, Germany

[2] Chair for Biological Imaging (CBI), Technische Universität München, Trogerstr. 9, 81675 Munich, and Institute for Biological and Medical Imaging (IBMI), Helmholtz Centre Munich, Ingolstaedter Landstraße 1, 85764 Oberschleißheim, Germany

[3] Department of Radiology, Leiden University Medical Center, Albinusdreef 2, 2333 ZA Leiden, The Netherlands

[4] Institute for Pathology, Klinikum rechts der Isar, Technische Universität München, Ismaningerstr. 22, 81675 Munich, Germany

[5] Department of Nuclear Medicine, Klinikum rechts der Isar, Technische Universität München, Ismaningerstr. 22, 81675 Munich, Germany

Downloaded from jnm.snmjournals.org by on October 29, 2018. For personal use only.

Synthesis

General

Protected amino acid analogs and 2-Chloro-tritylchloride polystyrene (2-CTC) resin (100-200 mesh; loading: 1.6 mmol/g) were purchased from Iris Biotech (Marktredwitz, Germany) or Bachem (Bubendorf, Switzerland). Fmoc-3-iodo-D-Tyrosine was obtained from Chemimpex (Wood Dale, IL, USA), and Sulfo-Cy5 free carboxylic acid was purchased from Lumiprobe GmbH (Hannover, Germany). All other organic reagents and solvents were from SigmaAldrich (Munich, Germany) or VWR (Ismaning, Germany). Solid phase peptide synthesis (SPPS) was carried out manually using an Intelli-Mixer syringe shaker (Neolab, Heidelberg). Analytical reversed-phase high performance liquid chromatography (RP-HPLC) was performed on a Nucleosil 100 C 18 (5µm, 125 x 4.0 mm) column (CS GmbH, Langerwehe, Germany) and preparative RP-HPLC using a Multospher 100 RP 18-5 (250 x 20 mm) column (CS GmbH, Langerwehe, Germany). Analytical RP-HPLC was performed on a Shimadzu Prominence HPLC system (Shimadzu Germany, Neufahrn, Germany) equipped with a diode array detector, and preparative RP-HPLC was performed on a Sykam gradient HPLC System (Sykam GmbH, Eresing, Germany) equipped with a 206 PHD UV-Vis detector (Linear^{TM} Instruments Corporation, Reno, USA). All compounds were eluted using linear gradients of acetonitrile (0.1% TFA, Solvent **B**) in 0.1 % TFA (v/v) (Solvent **A**) at a constant flow of 1 mL/min (analytical RP-HPLC) or 10 mL/min (semi-preparative purification). The specific gradients and retention times t_R are cited in the text.

Downloaded from jnm.snmjournals.org by on October 29, 2018. For personal use only.

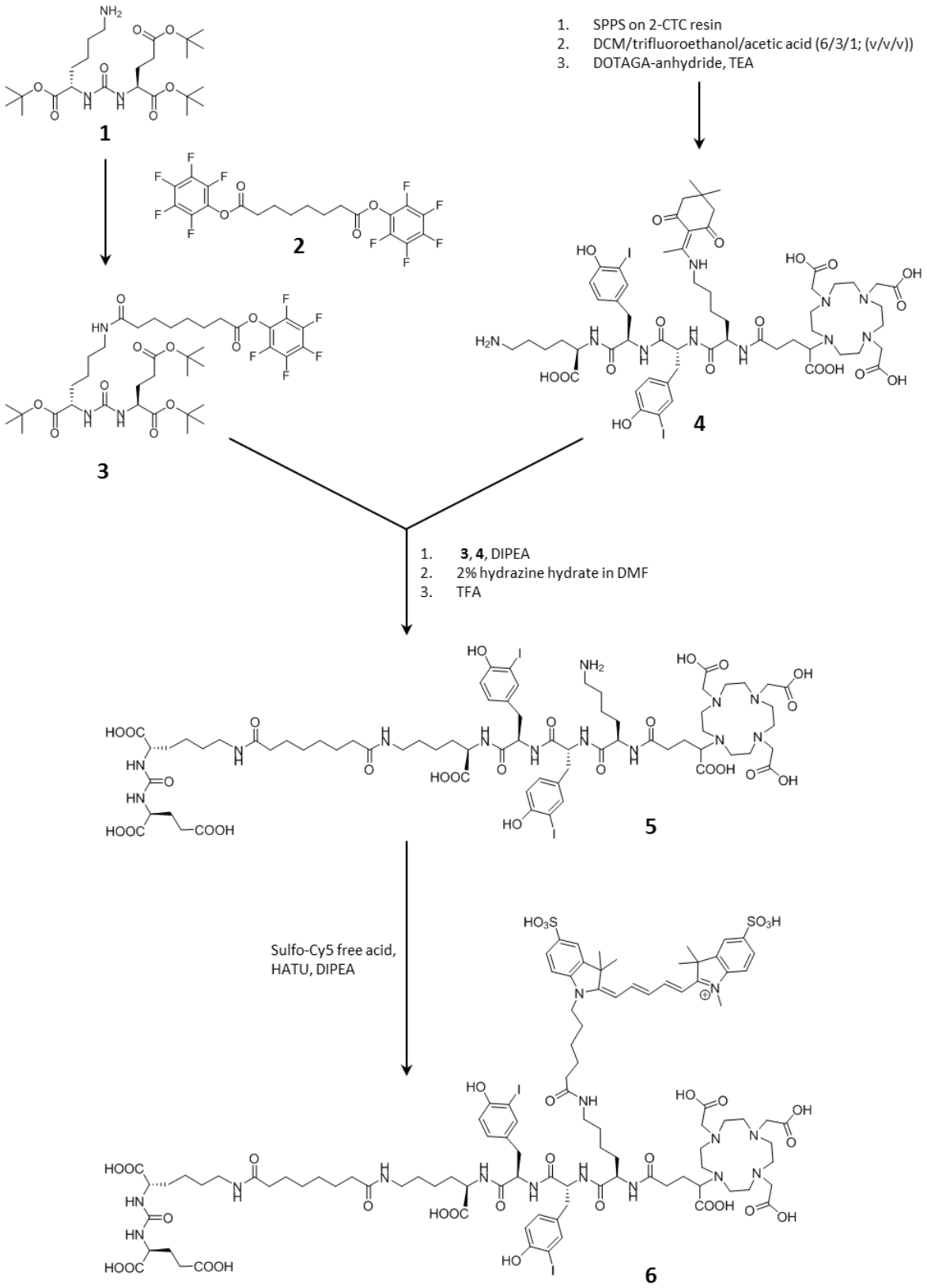

Supp. Fig. 1 *Synthesis Scheme for PSMA-I&F (**6**)*

Downloaded from jnm.snmjournals.org by on October 29, 2018. For personal use only.

*Synthesis of the carboxyl-protected Lys-urea-Glu (KuE) binding motif (**1**)*

The synthesis of *(tBu)KuE(tBu)$_2$* (**1**) was peformed as described previously (1,2).

HPLC (40-100% B in 15 min): t_R = 8.0 min

Calculated mass for **1** ($C_{24}H_{45}N_3O_7$): 487.6

ESI-MS : m/z = 488.4 $[M+H]^+$, 510.4 $[M+Na]^+$.

*Synthesis of the protected OPfp-Sub-KuE derivative (**3**)*

Sub(OPfp)$_2$ (**2**): Suberic acid (2.00 g, 11.5 mmol, 1 eq) was dissolved in 40 mL tetrahydrofurane (THF), and 2.78 mL (34.4 mmol, 3 eq) of pyridine and 7.12 mL (45.9 mmol, 4 eq) *N,N´*-diisopropylcarbodiimide (DIC) were added. To this mixture, a solution of pentafluorophenol (8.45 g, 45,9 mmol, 4 eq) in 12 mL THF was added. After stirring for 2 h at room temperature (RT), the solvent was evaporated *in vacuo* and the crude product was purified by silica gel column chromatography (Petroleum ether (PE)/Ethylacetate (EtOAc), 9/1, (v/v)) to yield **2** as a white crystalline solid (3.99 g; 68% yield).

HPLC (10-100% B in 15 min): t_R = 18.3 min.

OPfp-Sub-(tBu)KuE(tBu)$_2$ (**3**): A solution of **1** (341 mg, 700 µmol, 1 eq) and 239 µL *N,N*-diisopropylethylamine (DIPEA) (1.4 mmol, 2 eq) in 60 mL THF was added dropwise (within 30 min) to a cooled (0°C) solution of **2** (1.4 g, 2.8 mmol, 4 eq) in 20 mL THF. The mixture was then stirred for 2 h at RT. The solvent was evaporated to dryness and the crude product was purified via silica gel column chromatography (PE/EtOAc, 10% to 100 % EtOAc, (v/v)) to yield **3** as a white solid (377 mg; 68% yield).

HPLC (40-100% B in 15 min): t_R = 17 min

Calculated mass for OPfp-Sub-(tBu)KuE(tBu)$_2$ (**3**) ($C_{38}H_{56}F_5N_3O_{10}$): 809.39

ESI-MS : m/z = 810.4 $[M+H]^+$, 832.6 $[M+Na]^+$.

Synthesis of the peptidic spacer and DOTAGA functionalization

DOTAGA-D-Lys(Dde)-D-(3-iodo)Tyr-D-(3-iodo)Tyr-D-Lys-OH (DOTAGA-k(Dde)-(i-y)-(i-y)-k) (**4**):

Downloaded from jnm.snmjournals.org by on October 29, 2018. For personal use only.

Dry 2-CTC resin was suspended in a solution of Fmoc-D-Lys(Boc)-OH (2.8 eq with respect to reactive functional groups on the resin) and 3.75 eq of DIPEA in dry dichloromethane (DCM) under vigorous stirring. After 90 min at RT, 3 mL MeOH were added to cap unreacted tritylchloride groups of the resin. Subsequently, the resin was filtered, washed twice with DCM, DMF and MeOH and dried *in vacuo*, and the final loading of the resin with Fmoc-D-Lys(Boc)-OH was calculated. Solid-phase peptide synthesis of the peptide sequence was carried out using a standard Fmoc strategy in NMP using HOBt (1.5 eq) and TBTU (1.5 eq) as coupling reagents and DIPEA (4.5 eq) as a base. After final Fmoc-deprotection using 20% piperidine in DMF, the tetrapeptide linker was cleaved from the resin using a mixture of DCM/trifluoroethanol (TFE)/acetic acid (6/3/1; (v/v/v)) under retention of the acid labile Boc protecting group. Upon evaporation of the solvents *in vacuo*, and the crude dry peptide (H_2N-D-Lys(Dde)-D-(3-iodo)Tyr-D-(3-iodo)Tyr-D-Lys(Boc)-OH) was redissolved in DMF, and 2 eq of DOTAGA anhydride and 10 eq of triethylamine were added. Quantitative formation of the DOTAGA-conjugated peptide linker was usually obtained within 1 h at RT. The product was then precipitated using diethyl ether, washed and dried *in vacuo*. For Boc-deprotection, the peptide was redissolved in trifluoroacetic acid (TFA). After 10 min at RT, the deprotected peptide linker was precipitated using diethyl ether, washed and dried *in vacuo*.

HPLC (10-90% B in 15 min): t_R = 6.85 min

Calculated mass for DOTAGA-k(Dde)-(i-y)-(i-y)-k (**4**) ($C_{59}H_{84}I_2N_{10}O_{18}$): 1474.4

ESI-MS : m/z = 1475.6 $[M+H]^+$, 738.6 $[M+2H]^{2+}$

*Conjugation of DOTAGA-k(Dde)-(i-y)-(i-y)-k with the KuE binding motif and deprotection (**5**)*

To a solution of **4** (82 mg, 56 µmol, 1 eq) and Triethylamine (TEA) (60 µL, 420 µmol, 7.5 eq) in 500 µL DMF, a solution of 50 mg **3** (62 µmol, 1.1 eq) in 250 µL DMF was added The reaction mixture was stirred for 1h at RT, and quantitative product formation was confirmed using RP-HPLC.

HPLC (10-90% B in 15 min): t_R = 10.84 min

Calculated mass for DOTAGA-k(Dde)-(i-y)-(i-y)-k-Sub-(tBu)KuE(tBu)$_2$ ($C_{91}H_{130}I_2N_{13}O_{27}$): 2101.0

Downloaded from jnm.snmjournals.org by on October 29, 2018. For personal use only.

ESI-MS : m/z = 1051.0 $[M+2H]^{2+}$

For *in situ* Dde-deprotection, 40 µl of hydrazine hydrate were added to the reaction mixture. After 10 min at RT, the crude product was precipitated using diethyl ether, washed and dried *in vacuo*.

HPLC (10-90% B in 15 min): t_R = 9.77 min

Calculated mass for DOTAGA-k-(i-y)-(i-y)-k-Sub-(tBu)KuE$(tBu)_2$ ($C_{81}H_{127}I_2N_{13}O_{25}$): 1936.8

ESI-MS : m/z = 1936.6 $[M+H]^+$, 968.8 $[M+2H]^{2+}$

For removal of remaining tBu-protecting groups, crude DOTAGA-k-(i-y)-(i-y)-k-Sub-K(tBu)-u-E$(tBu)_2$ was then dissolved in 1 mL of TFA. After 45 min at RT, the fully deprotected product DOTAGA-k-(i-y)-(i-y)-k-Sub-KuE (**5**) was precipitated using diethyl ether and purified using semipreparative RP-HPLC.

HPLC (10-90% B in 15 min): t_R = 5.93 min

Calculated mass for DOTAGA-k-(i-y)-(i-y)-k-Sub-KuE (**5**) ($C_{69}H_{103}I_2N_{13}O_{25}$): 1768.5

ESI-MS : m/z = 1769.2 $[M+H]^+$, 884.7 $[M+2H]^{2+}$

*Conjugation with Sulfo-Cy5 (**6**)*

Sulfo-Cy5 free acid (3 mg, 4.5 µmol) and HATU (2.6 mg, 6.75 µmol, 1.5 eq) were dissolved in 200 µL DMF, and 2.3 µL DIPEA (13.5 µmol, 3 eq) were added. The mixture was allowed to stand at RT for 5 min and was then slowly added to a solution of **5** (8.8 mg, 5 µmol, 1.1 eq) in 200 µL of DMF. After 20 min at RT, quantitative reaction was confirmed using RP-HPLC. The final product PSMA-I&F (DOTAGA-k(Sulfo-Cy5)-(i-y)-(i-y)-k-Sub-KuE, **6**) was purified using semipreparative RP-HPLC (3.3 mg, 28% yield based on DOTAGA-k-(i-y)-(i-y)-k-Sub-KuE).

HPLC (15-45% B in 15 min): t_R = 10.79 min

Calculated mass for PSMA-I&F (**6**) ($C_{101}H_{140}I_2N_{15}O_{32}S_2$): 2392.7

ESI-MS : m/z = 1197.7 $[M+2H]^{2+}$, 798.4 $[M+3H]^{3+}$

Downloaded from jnm.snmjournals.org by on October 29, 2018. For personal use only.

The ^{nat}Ga- and ^{nat}Lu-complexes of PSMA-I&F were prepared by dissolving 200-500 µg of peptide either in 20 mM $GaNO_3$ or $LuCl_3$ in 0.01 M HCl to yield a final peptide concentration of 1 mM. After heating to 95°C for 30 minutes in a sealed tube, RP-HPLC analysis revealed quantitative complex formation. The product solutions were used as such for the preparation of dilution series for binding or internalization studies.

Calculated mass for Ga-PSMA-I&F ($C_{101}H_{138}I_2N_{15}O_{32}S_2Ga$): 2459.7

ESI-MS : m/z = 1230.5 $[M+2H]^{2+}$, 820.8 $[M+3H]^{3+}$

Calculated mass for Lu-PSMA-I&F ($C_{101}H_{137}I_2N_{15}O_{32}S_2Lu$): 2564.7

ESI-MS : m/z = 1283.6 $[M+2H]^{2+}$, 856.0 $[M+3H]^{3+}$

Downloaded from jnm.snmjournals.org by on October 29, 2018. For personal use only.

Radiolabeling

^{68}Ga-labeling

The non-processed eluate of a ^{68}Ge/^{68}Ga-generator with SnO_2 matrix (by IThemba LABS, SA; 1.25 mL, eluent: 1 M aq. HCl, total ^{68}Ga activity: 500 MBq) was adjusted to pH 2 by adding HEPES buffer (950 µL of a 2.7 M aq. solution) and used for labelling of 5.0 nmol of PSMA-I&F for 5 minutes at 95 °C. The labeled product was isolated by passing the reaction mixture through a C8 light solid phase extraction cartridge (SepPak), which was then purged with water (10 mL), followed by elution of 68Ga-PSMA-I&F using 2 mL 50% aqueous ethanol. After removal of the organic solvent *in vacuo*, the product solution was diluted with PBS to the desired activity concentration for use in the *in vitro* and *in vivo* studies.

^{177}Lu-labeling

For ^{177}Lu-labeling according to a standard procedure (3), PSMA-I&F was dissolved in DMSO to yield a 1 mM solution. Of this solution, the required volume was added to $^{177}LuCl_3$ in 0.04 M HCl (ITG/ITM, Garching, Germany; activity concentration: 370 MBq/500 µl) to achieve a precursor-to-^{177}Lu-activity ratio of 1 nmol precursor per 225 MBq $^{177}LuCl_3$. To this mixture, 1 M NH_4OAc was added (calculated to be 10% of total reaction volume), and the mixture was heated to 95°C for 20 min. After cooling and determination of the radiochemical purity (usually >98%), the reaction mixture was diluted with PBS to the desired activity concentration and used as such for *in vitro* and *in vivo* studies.

Radiochemical purity of ^{68}Ga-PSMA-I&F and [^{177}Lu]PSMA-I&F was determined using radio-TLC. Radio-TLC was carried out using Agilent iTLC silica gel impregnated chromatography paper (Agilent, Waldbronn, Germany) and two different mobile phases, i.e. A) 0.1 M aq. sodium citrate and B) a 1:1 (v/v) mixture of 1 M aq. NH_4OAc and MeOH. TLC-strips were analyzed using a Bioscan TLC analyzer.

Downloaded from jnm.snmjournals.org by on October 29, 2018. For personal use only.

In vitro evaluation

Cell culture

PSMA overexpressing LNCaP (human prostate carcinoma) cells were grown in DMEM/Nutrition Mix F-12 with Glutamax-I (1:1) (Invitrogen, Life Technologies, Darmstadt, Germany) supplemented with 10% FCS. For IC_{50} determination, approximately 150.000 cells/well were seeded on 24-well plates one day prior to the experiment. For internalization studies, 125.000 cells/well in PLL-coated 24-well plates were used. Cell counting was carried out using a Countesse automated cell counter (Invitrogen, Carlsbad, USA).

Internalization studies

LNCaP cells were incubated with the respective radioligands for different time points up to 120 min at 37°C. The supernatant was removed, cells were washed with assay medium, and an acid wash (50 mM NaOAc in saline, pH 4.5) was performed to remove membrane-associated activity. Cells were then lysed using 1N NaOH, and internalized activity was quantified using a γ-counter. Data were corrected for non-specific internalization in the presence of 10 µM 2-PMPA (2-(Phosphonomethyl)pentane-1,5-dioic acid; Tocris Bioscience, Bristol, UK) and normalized to the specific internalization observed for the radioiodinated reference compound in the same experiment. Data represent means ± SD (n=3).

Fluorescence microscopy

LNCaP cells (100.000 cells/well) were seeded in 24 well plates on glass cover slips (12 mm diameter) one day before the microscopy experiment. On the next day, the culture medium was replaced by incubation medium (DMEM (5% BSA)), and the adherent cells were incubated with the respective PSMA-I&F analog (100 or 25 nM) in the absence (total binding/internalization) or presence (non-specific binding/internalization) of 10 µM 2-PMPA at 37 °C for 5 min or 60 min. Hoechst 33342 (final concentration: 2 µg/ml) and LysoTracker Green (Life technologies, Carlsbad, California; final concentration: 100 nM) were

Downloaded from jnm.snmjournals.org by on October 29, 2018. For personal use only.

added 2 min before the end of incubation. To end incubation, the cover slips were removed from the incubation medium, washed with PBS and fixed in 4 % Histofix solution.

Microscopy was performed on a Keyence BZ-9000 fluorescence microscope equipped with Cy5 (620/60 nm excitation, 700/75 nm emission), DAPI-BP (370/50 nm excitation, 447/60 nm emission) and GFP-BP (472.5/30 nm excitation, 520/35 nm emission) filters. Images were processed using the BZ-9000 analyzer software.

Downloaded from jnm.snmjournals.org by on October 29, 2018. For personal use only.

In vivo Evaluation

Tumor model

To induce tumor growth, a suspension of LNCaP cells (approx. 5 x 10^6 cells/mouse) in 200 µl of a 1:1 mixture of serum-free DMEM and Matrigel (BD Biosciences) was injected subcutaneously into the right shoulder of male SCID Hairless Outbred (SHO) mice (Charles River Laboratories, Sulzfeld, Germany). After 2-4 weeks, tumor size reached 4-8 mm in diameter and the mice were used for the in vivo studies.

Histopathology and PSMA immunohistochemistry

Mouse tissues were fixed in 10% neutral-buffered formalin solution for min. 48 h, dehydrated under standard conditions (Leica ASP300S, Wetzlar, Germany) and embedded in paraffin. Serial 2µm-thin sections prepared with a rotary microtome (HM355S, ThermoFisher Scientific, Waltham, USA) were collected and subjected to histological and immunohistochemical analysis. Hematoxylin-Eosin (H.-E.) staining was performed on deparaffinized sections with Eosin and Mayer's Haemalaun according to a standard protocol. Immunohistochemistry was performed using a BondMax RXm system (Leica, Wetzlar, Germany, all reagents from Leica) with a primary antibody against PSMA (abcam, Cambridge, UK, ab133579, diluted 1:100 in antibody diluent). Briefly, slides were deparaffinized using deparaffinization solution, pretreated with Epitope retrieval solution 1 (corresponding to citrate buffer pH=6) for 20 minutes. Antibody binding was detected with a polymer refine detection kit without post primary reagent and visualized with DAB as a dark brown precipitate. Counterstaining was done with hematoxyline. Murine organs and tumor tissue were evaluated by an experienced pathologist (KS). PSMA expression intensity was scored using a 4-tier score (0= absent, 1= slight, 2= moderate, 3= intense).

Downloaded from jnm.snmjournals.org by on October 29, 2018. For personal use only.

Ex vivo Evaluation

Whole-body cryosectioning and fluorescence imaging

A LNCaP xenograft bearing SHO mouse (the same animal that had been used for the static PET scan two days previously) was injected with 2 nmol of ^{nat}Ga-PSMA-I&F, sacrificed at 1h p.i., embedded in a mixture of Tissue-Tek and black ink (7.41% v/v) inside a cylinder of 3.5 cm diameter, and placed into the -80°C freezer overnight. Before sectioning the specimen was placed into the cryostat at -17°C for two hours.

Cryosections were prepared using a Leica CM 3500 cryostat (Leica, Wetzlar, Germany) at a slice thickness of 20 µm. The temperature during slicing was adjusted to -17°C. A highly sensitive fluorescence imaging system was mounted onto the cryostat and imaged the specimen after every 4 slices. The imaging protocol consisted of the acquisition of three reflectance images at 630/60 nm (red channel), 535/38 nm (green channel), and 460/50 nm (blue channel) for color imaging and one fluorescence image at 670/10 nm, which is close to the maximum emission of the sulfo-Cy5 (i.e. 662 nm). We employed a halogen light source (KL2500, Schott, New York, USA) coupled to fiber bundles and a motorized filter-wheel (FW102C, Thorlabs, New Jersey, USA) to illuminate the specimen. Reflectance images were enabled by white-light illumination (i.e. no light source filtering), whereas bandpass filter (ET620/60X, Chroma Technology, Rockingham, Vermont, United States) was placed in the filter-wheel to enable sulfo-Cy5 excitation.

Images were recorded by an iXon electron multiplying charge-coupled device (EMCCD, DV8201-BV, Andor Technology, Belfast, Northern Ireland). A Leica Z16 Apo Macroscope was coupled to the camera, allowing manual adjustments of zoom, focus, and fields of view (FOV). In the lens-camera path a 25-positions filter-wheel was placed with mounted three bandpass filters (D630/60M, D535/38M, and D460/50X, Chroma Technology) for reflectance acquisition and one bandpass filter (D670/10X, Chroma Technology) for fluorescence acquisition. Supp. Fig. 1 depicts a schematic of the system.

The serial sectioning and imaging system was fully automated using custom software implemented in LabView (National Instruments, Austin, USA) to control sectioning and trigger image acquisition (4). Gain

Downloaded from jnm.snmjournals.org by on October 29, 2018. For personal use only.

of the EMCCD was maintained constant during sectioning at 2, 10 and 20 for the red, green and blue channels, and at 300 for fluorescence imaging, while exposure time was automatically adjusted per imaged slice and ranged from 0.001 s to 20 s depending on the per slice amount of the reflected or emitted light. Post-processing involved normalization of the acquired data to their corresponding exposure time, reconstruction of the color images from the red, green, and blue channels, and longitudinal alignment of the three-dimensional stack of imaged slices for optimal resolution. These processes were implemented in MATLAB (Mathworks, Natick, USA), while Amira (FEI Visualization Sciences Group, Burlington, USA) was used for cross-sectional and longitudinal visualization of the acquired data, and three-dimensional representation of the fluorescence data.

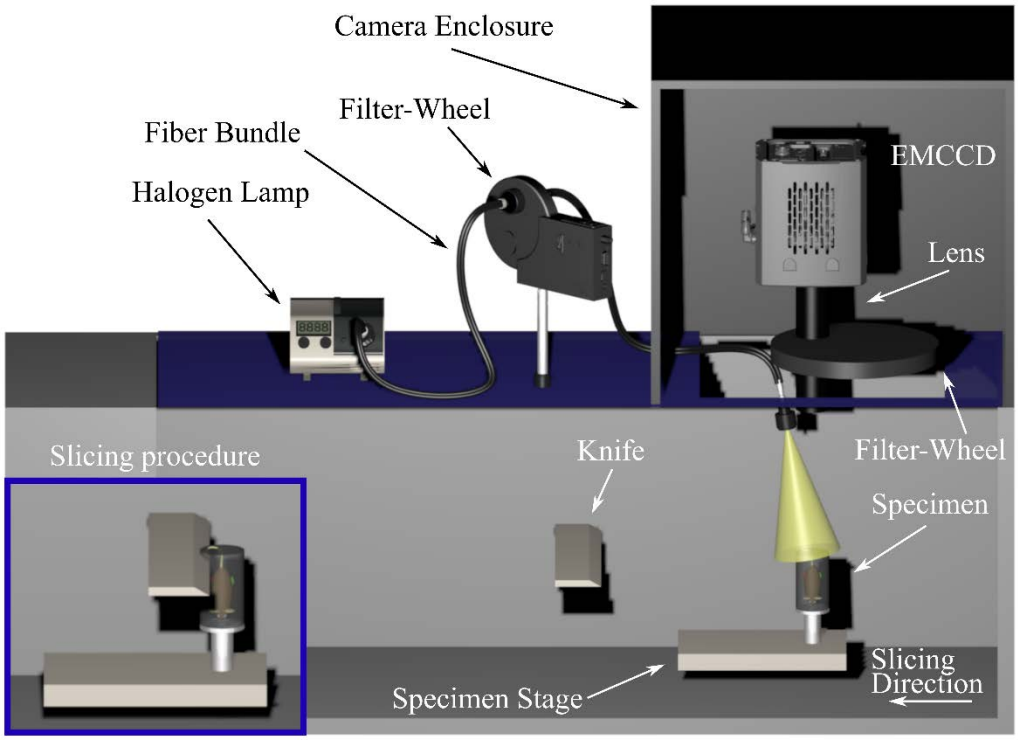

Supp. Fig. 2. *The serial sectioning and imaging system. A halogen lamp is employed to deliver illumination onto the imaged specimen. Reflectance and fluorescence images are acquired by a highly sensitive electron multiplying charge-coupled device (EMCCD) at specific spectral bands defined by filter-wheels at both the excitation and detection illumination paths. Left inset depicts the slicing procedure, which is repeated 4 times with a step of 20 μm before imaging the sample (resulting to 80 μm imaging step). All CAD optomechanical components are courtesy of Thorlabs (www.thorlabs.com).*

Downloaded from jnm.snmjournals.org by on October 29, 2018. For personal use only.

Intraoperative fluorescence imaging

Fluorescence imaging (intraoperative/ex vivo) of LNCaP xenografts in CB17-SCID mice (1h p.i.) was performed using two different instrumental setups. First, a Dino-lite handheld digital microscope for Cy5 (Dino-Lite Edge AM4115T-DFRW, AnMo Electronics Corporation, Hsinchu, Taiwan) was used. Acquisition was performed at $\lambda_{ex\,max}$ 620 nm, and $\lambda_{em\,max}$ 650 nm and at a magnification range of 20-220x. Images were captured using DinoCapture 2.0 software (AnMo Electronics Corporation). Second, a 0° Firefly laparoscope that is compatible with the surgical robotic da Vinci Si system (Intuitive Surgical Inc., Sunnyvale, California, USA) was employed. For excitation, the red light-emitting diode (LED) ($\lambda_{ex\,max}$ at 636 nm) of the Firefly light source was isolated using LED-controller software provided by Intuitive Surgical. For practical reasons, a Karl Storz fluid light cable was used to illuminate the target (495 FR; KARL STORZ Endoskope GmbH & Co. KG, Tuttlingen, Germany). An Edmund Optics bandpass filter (center wavelength $\lambda_{em\,max}$ 692 nm, full width at half maximum 47 nm; Edmund Optics Inc., Barrington, NJ, USA) was used to isolate the Cy5 emission. Images were captured from the unprocessed Firefly video feed.

Downloaded from jnm.snmjournals.org by on October 29, 2018. For personal use only.

RESULTS

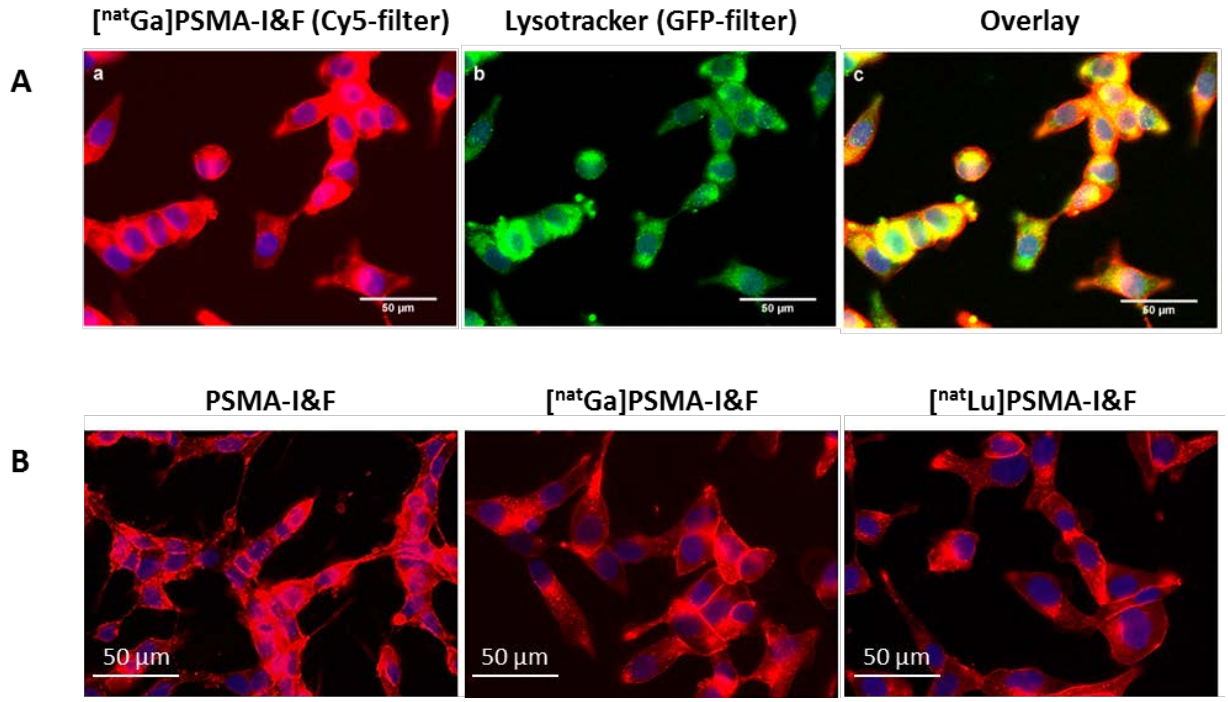

Supp. Fig. 3 ***A)*** *Fluorescence microscopy of the internalization of [natGa]PSMA-I&F (100 nM) into LNCaP prostate carcinoma cells after 60 min at 37°C (a) (Cy5-filter; overlay with nuclear blue fluorescence acquired using the DAPI filter (Hoechst 33342)). Images acquired using the GFP filter show uptake of the lysosomal dye LysoTracker (b). An overlay of all three channels is shown on the right (c).*
B) *Fluorescence microscopy of the internalization of PSMA-I&F (free DOTAGA), [natGa]PSMA-I&F and [natLu]PSMA-I&F (25 nM) into LNCaP prostate carcinoma cells after 60 min at 37°C.*

1. Weineisen M, Simecek J, Schottelius M, Schwaiger M,Wester HJ. Synthesis and preclinical evaluation of DOTAGA-conjugated PSMA ligands for functional imaging and endoradiotherapy of prostate cancer. *EJNMMI research.* 2014;4:63.
2. Robu S, Schottelius M, Eiber M, Maurer T, Gschwend J, Schwaiger M, et al. Preclinical Evaluation and First Patient Application of 99mTc-PSMA-I&S for SPECT Imaging and Radioguided Surgery in Prostate Cancer. *J Nucl Med.* 2017;58:235-242.
3. Breeman WA, De Jong M, Visser TJ, Erion JL,Krenning EP. Optimising conditions for radiolabelling of DOTA-peptides with 90Y, 111In and 177Lu at high specific activities. *Eur J Nucl Med Mol Imaging.* 2003;30:917-920.
4. Symvoulidis P, C. C. Perez, Schwaiger M, Ntziachristos V,Westmeyer GG, Serial sectioning and multispectral imaging system for versatile biomedical applications. In *2014 IEEE 11th International Symposium on Biomedical Imaging (ISBI)*, 2014; pp 890-893.

Downloaded from jnm.snmjournals.org by on October 29, 2018. For personal use only.

The Journal of NUCLEAR MEDICINE

Synthesis and preclinical characterization of the PSMA-targeted hybrid tracer PSMA-I&F for nuclear and fluorescence imaging of prostate cancer

Margret Schottelius, Alexander Wurzer, Katharina Wissmiller, Roswitha Beck, Maximilian Koch, Dimitrios Gkorpas, Johannes Notni, Tessa Buckle, Matthias N. van Oosterom, Katja Steiger, Vasilis Ntziachristos, Markus Schwaiger, Fijs W.B. van Leeuwen and Hans-Jürgen Wester

J Nucl Med.
Published online: September 20, 2018.
Doi: 10.2967/jnumed.118.212720

This article and updated information are available at:
http://jnm.snmjournals.org/content/early/2018/09/20/jnumed.118.212720

Information about reproducing figures, tables, or other portions of this article can be found online at:
http://jnm.snmjournals.org/site/misc/permission.xhtml

Information about subscriptions to JNM can be found at:
http://jnm.snmjournals.org/site/subscriptions/online.xhtml

JNM ahead of print articles have been peer reviewed and accepted for publication in *JNM*. They have not been copyedited, nor have they appeared in a print or online issue of the journal. Once the accepted manuscripts appear in the *JNM* ahead of print area, they will be prepared for print and online publication, which includes copyediting, typesetting, proofreading, and author review. This process may lead to differences between the accepted version of the manuscript and the final, published version.

The Journal of Nuclear Medicine is published monthly.
SNMMI | Society of Nuclear Medicine and Molecular Imaging
1850 Samuel Morse Drive, Reston, VA 20190.
(Print ISSN: 0161-5505, Online ISSN: 2159-662X)

© Copyright 2018 SNMMI; all rights reserved.

SNMMI SOCIETY OF NUCLEAR MEDICINE AND MOLECULAR IMAGING